Energy 331 (2025) 136563

Contents lists available at ScienceDirect

Energy

journal homepage: www.elsevier.com/locate/energy

Comprehensive energy, economic, and environmental analysis of a hybrid photovoltaic–thermal (PVT) heat pump system

Hugo Arnesson [a], Andreas V. Olympios [b,c], Asmaa A. Harraz [d], Jingyuan Xu [a,*]

[a] Institute for Microstructure Technology, Karlsruhe Institute of Technology, Hermann-von-Helmholtz-Platz 1, 76344, Eggenstein-Leopoldshafen, Germany
[b] PV Technology Laboratory, Department of Electrical and Computer Engineering, University of Cyprus, Nicosia, Cyprus
[c] PHAETHON Centre of Excellence for Intelligent, Efficient and Sustainable Energy Solutions, Nicosia, Cyprus
[d] Environmental Engineering Program, University of Science and Technology, Zewail City of Science and Technology, Egypt

ARTICLE INFO

Keywords:
Solar-assisted heat pump
Energy–economic–environmental (3E)
Photovoltaic–thermal (PVT)
Propane refrigerant
R32 refrigerant

ABSTRACT

This study investigates a parallel indirect-expansion solar-assisted heat pump (SAHP) system integrating photovoltaic–thermal (PVT) collectors to meet domestic space heating, hot water, and appliance electricity demands for a typical household in Germany. A transient mathematical model captures the interdependencies between heat and electricity flows, enabling evaluation of thermodynamic, economic, and environmental performance across 54 heat pump designs with 3 refrigerants. The SAHP is compared to standalone heat pumps and natural gas boilers under varying electricity and natural gas prices. Results indicate that the SAHP system can cover over one-third of annual heating demand and half of appliance electricity demand using solar energy, with Munich achieving the highest solar coverage (39 %). HFC-32 (R32) outperforms propane, which in turn outperforms R410A, with levelized costs of energy, in electricity equivalents, of 0.272, 0.276 and 0.283 Euro/kWh, respectively. The SAHP system proves more cost-effective than standalone heat pumps or natural gas boilers unless energy prices are exceptionally low. Optimizing water tank designs for lower-temperature operation could further enhance SAHP competitiveness against PV-driven heat pumps.

1. Introduction

Greenhouse gas (GHG) emissions, primarily carbon dioxide, continue to rise due to human activities, with electricity and heat generation contributing nearly one-third of global emissions in 2019 [1]. Within the EU, the heating and cooling sector holds significant importance, accounting for nearly 50% of final energy consumption. Despite this, decentralized fossil-based technologies, such as gas boilers, remain the dominant heating method in Europe, with fossil fuels comprising 80% of the heating and cooling sector's energy mix [2]. Efforts to reduce this dependency are underway. Notably, the 2023 revision of the Energy Performance of Buildings Directive aims for carbon neutrality in all buildings by 2050, mandating carbon neutrality for new buildings as early as 2028 [3].

Heat pumps (HPs) are pivotal in the decarbonization of heating and are rapidly gaining popularity. Within the EU, the HP sector has already become the largest contributor to the growth of renewable energy production in the heating and cooling sector [2]. Similarly, solar technologies play an essential role in the transition to cleaner energy sources. Solar thermal (ST) technologies directly harness the sun's heat for use, while photovoltaic (PV) technologies generate clean electricity to power electrified heating systems, including HPs. Together, these technologies support the shift toward sustainable heating solutions.

Solar-assisted heat pumps (SAHPs) integrate HPs with solar energy technologies, reducing the electrical workload and lowering emissions compared to standalone HPs [2]. Current state-of-the-art SAHP systems encompass various configurations that have been extensively studied and are beginning to penetrate the heating market [4]. SAHPs can be categorized based on three key characteristics: the type of solar technology utilized, ST or photovoltaic–thermal (PVT); the circulation method of the heat transfer fluid (HTF), direct-expansion (DX) or indirect-expansion (IDX); and the system configuration, parallel, serial, or dual source [4].

Using PVT instead of ST collectors can increase the share of renewable energy in domestic SAHP systems and ensure good performance and reliability [5]. Novel research suggesting a covered PVT-SAHP system, concludes that electrical efficiencies surpass those of traditional PV modules for the same conditions because of the cooling effect offered by the solar HTF on the PVT modules [6]. Additionally, a study showed PVT SAHPs show better performances in terms of primary energy consumption in comparison to ST SAHP or standalone HPs [7].

* Corresponding author.
E-mail address: jingyuan.xu@kit.edu (J. Xu).

https://doi.org/10.1016/j.energy.2025.136563
Received 5 March 2025; Received in revised form 23 April 2025; Accepted 12 May 2025
Available online 29 May 2025

Nomenclature

Abbreviations

COP	Coefficient of performance
DX	Direct-expansion
ETS	Emission trading system
GWP	Global warming potential
HEX	Heat exchanger
HE	High electrical
HP	Heat pump
HTF	Heat transfer fluid
HWD	Hot water demand
IDX	Indirect-expansion
MPP	Maximum power point
NTU	Number of transfer units
PPTD	Pinch point temperature difference
PVT	Photovoltaic thermal
PV	Photovoltaic
SAHP	Solar-assisted heat pump
SFH	Single-family house
SHD	Space heating demand
ST	Solar thermal

Variables

α	Absorptivity, dimensionless
β	Temperature coefficient of MPP power, in K^{-1}
ΔP	Pressure drop, in Pa
$\dot{m}$	Mass flow rate, in kg/s
$\dot{Q}$	Heat flow rate, in W
η	Efficiency, dimensionless
ρ	Density, in kg/m^3
σ	Stefan–Boltzmann constant, in W/m^2/K^4
ε	Emissivity, dimensionless
A	Area, in m^2
a_1	First-order heat loss coefficient, in W/m^2 K
a_2	Second-order heat loss coefficient, in W/m^2 K^2
C	Costs, in Euro
c	Energy purchase price, in Euro/kWh
c_p	Specific heat capacity, in J/kg K
CS	Cost savings, in Euro
d	Discount rate, dimensionless
D_h	Hydraulic diameter of the pipes, m^2
E	Electrical energy, in kWh
$EPCS$	Environmental penalty cost savings, in Euro
ER	Emission reduction, in kgCO_2
f	Emission factor, in kgCO_2/kWh
G	Incident irradiance, in W/m^2
h	Heat transfer coefficient, in W/m^2/K
I	Initial investment, in Euro
i_f	Inflation, dimensionless
k	Thermal conductivity, in W/m K
L	Length, in m
$LCOE$	Levelized cost of energy, in Euro/kWh
M	Mass, in kg
n	Investment horizon, in years
NPV	Net present value, in Euro
P	Power, in W
PBT	Payback time, in years
Q	Thermal energy, in kWh
R	Thermal resistance, in W/m^2 K
r	Radius, m
s	Energy selling price, in Euro/kWh
T	Temperature, in °C
t	Time, in s
U	Overall heat transfer coefficient, in W/m^2 K

Subscripts

0	Optical
app	Appliances and lighting
aux	Auxiliary
a	Ambient
conv	Convective
cov	Covered
el	Electrical
eq, el	Electricity equivalents
exc	Excess
e	Electricity
HW	Hot water
ins	Insulation
i	Inner
lim	Limit
MF	Mean fluid
mod	Module
ng	Natural gas
O&M	Operation and maintenance
o	Outer
prod	Production
ref	Reference
SH	Space heating
th	Thermal
uncov	Not covered
u	Absorbed
WT	Water tank

In DX SAHPs, ST or PVT collectors function as evaporators, eliminating the need for a separate solar loop. In contrast, IDX systems require a solar and HP loop, connected either in series or parallel. The literature does not present any comparative studies between DX and IDX SAHPs, either experimentally or through modeling [8]. However, the advantages of each configuration can be summarized. DX systems require fewer components and reduce the risk of evaporator frosting in the HP, but the ST collectors in these systems are susceptible to heat losses to the ambient when overheated [8,9]. On the other hand, IDX systems feature insulated ST collectors, minimizing heat losses while also offering improved stability and ease of control at the expense of higher complexity [8,10].

In IDX systems with a series connection, a heat exchanger (HEX) acts as the evaporator, linking the solar and HP loops. In a parallel configuration, the solar and HP loops operate independently [8]. Among all SAHP configurations, the IDX parallel configuration is considered the most practical and commercially viable [4]. A study comparing different types of IDX SAHPs, including parallel and serial configurations, found that the parallel IDX SAHP could achieve significantly higher seasonal performance factors than a typical air-source HP [11].

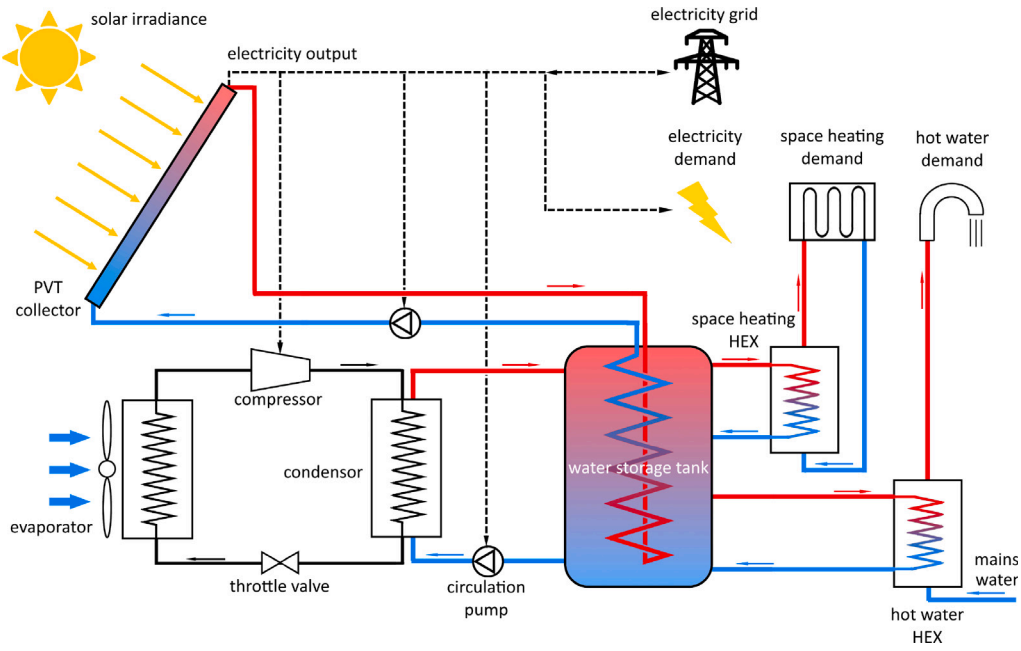

Fig. 1. Schematic of the investigated solar-assisted heat pump system.

Research suggests that when air serves as the parallel heat source, this configuration outperforms serial configurations, delivering higher annual average coefficients of performance (COP) and reducing overall energy consumption [12]. Furthermore, the benefits of serial SAHP configurations are less pronounced in colder climates, making parallel configurations more advantageous under diverse conditions [13]. Simulation models of parallel IDX SAHPs have been developed and experimentally validated, demonstrating their energy efficiency as an alternative for space and water heating compared to traditional boilers or HPs [14,15].

The applications of SAHPs include water and space heating in both residential and commercial environments [16]. Some studies also explore the potential for space cooling using the same system. A ground-source SAHP, capable of providing both heating in winter and cooling in summer by leveraging stable deep-ground temperatures, could lead to significant electricity and CO_2 emission savings [17–19]. Another promising application of SAHPs is drying, relevant in agriculture, commerce, construction, and housing. Compared to standalone HPs, SAHPs not only enhance energy savings but also offer advantages such as higher drying rates and superior quality dried products [20,21].

Most existing modeling studies on SAHPs primarily focus on energy analysis, while comprehensive evaluations integrating energy, economic, and environmental aspects are limited to a handful of studies. Considering that the high cost of SAHPs remains a significant barrier to widespread adoption, economic analysis is particularly crucial [4,9]. Additionally, a key research gap lies in the role of HP design within SAHP systems [21]. The performance of different HP designs varies significantly depending on operating conditions and refrigerant types, yet this area has not been extensively explored.

This study seeks to bridge gaps in the existing literature by examining an IDX parallel SAHP system integrated with a PVT array through a transient model developed in MATLAB, and a HP design model. The novelty of the methodology developed in this work is threefold. First, the study analyses and establishes the feasibility of the IDX parallel SAHP configuration through comprehensive economic, environmental, and thermodynamic performance modeling, a perspective not found in previous literature for this specific SAHP configuration. Second, the study utilizes detailed component-level techno-economic models to systematically evaluate a comprehensive set of 54 potential distinct HP designs, incorporating three commonly used refrigerants representative of state-of-the-art systems. For each HP model the SAHP performance is assessed, providing a level of technical detail that is a significant contribution to current research. Third, the work includes a comprehensive and holistic comparison of the SAHP system against alternative conventional heating technologies, including standalone HPs and natural gas boilers, under varying economic conditions. This comparative analysis offers insights into the competitiveness of the proposed system across various market scenarios.

Germany, with its high dependence on fossil fuels and significant growth in installed solar technologies, is chosen as the case study, focusing on the residential sector, which accounts for 54% of heating and cooling demand in the EU [2], through an examination of a single-family house (SFH).

2. Methodology

2.1. Solar systems description

The studied SAHP system features an indirect-expansion, parallel configuration. The storage tank is heated via two separate loops: the PVT collector loop, utilizing a submerged coil, and the HP loop, employing an external HEX. The storage tank serves dual purposes, meeting both hot water demand (HWD) and space heating demand (SHD) through two additional HEXs. The system schematic is illustrated in Fig. 1.

2.1.1. Photovoltaic thermal (PVT) collectors

The PVT modules heat the solar HTF, which is water in this study [22]. When sufficiently warm, the water is circulated through the tank coil for heat transfer. The cooled HTF is then pumped back to the thermal components for reheating. The amount of heat absorbed by the PVT collectors is determined by the thermal efficiency, which allows for the calculation of the outlet and inlet temperatures of the circulating water within the PVT array.

The thermal efficiency is calculated according to the ISO 9806:2017 standard for solar thermal collectors, expressed as a second-order function of the temperature difference between the mean fluid temperature T_{MF}, and the ambient temperature, T_a, as shown in Eq. (1) [23,24]:

$$\eta_{th} = \eta_0 - a_1\left(\frac{T_{MF}-T_a}{G}\right) - a_2 G\left(\frac{T_{MF}-T_a}{G}\right)^2, \quad (1)$$

where η_0 is the optical efficiency, a_1 is the first-order heat loss coefficient, a_2 is the second-order heat loss coefficient that accounts for the quadratic heat loss variation, and G is the incident irradiance.

The heat transfer from the PVT circulation water to the water tank in the coil is obtained with the effectiveness of the coil in Eq. (2) [25]:

$$\dot{Q}_{\mathrm{PVT}} = \varepsilon_{\mathrm{HEX1}} \dot{Q}_u, \tag{2}$$

where $\dot{Q}_{\mathrm{PVT}}$ is the heat transferred from the circulating water to the water tank, $\varepsilon_{\mathrm{HEX1}}$ is the HEX effectiveness, and $\dot{Q}_{\mathrm{u}}$ is the heat absorbed from solar energy in the PVT collectors. Applying the number of transfer units (NTU) method to a single-stream HEX gives Eq. (3) [25]:

$$\varepsilon_{\mathrm{HEX1}} = 1 - e^{\text{-NTU}}. \tag{3}$$

The PVT module also generates electricity, and the distribution of this electricity to its various uses follows this order of priority: powering the pump in the PVT water circulation system, supplying appliances and lighting, powering the HP, and finally, selling excess power to the grid. The power consumption of the circulation pumps is detailed in Appendix A. Since their consumption is minimal, it is aggregated with the power usage of the appliances. Grid electricity complements the power requirements during periods of reduced solar irradiation. The electrical power generated in the PVT array is determined by the electrical efficiency of the module which is modeled in Eq. (4), using maximum power point (MPP) tracking. The equation allows to determine the efficiency at a given irradiance and module temperature from an efficiency at reference conditions [26]:

$$\eta_{\mathrm{el}}(G, T_{\mathrm{mod}}) = \eta_{\mathrm{el}}(G_{\mathrm{ref}}, T_{\mathrm{ref}})(1 + \beta(T_{\mathrm{mod}} - T_{\mathrm{ref}})), \tag{4}$$

where η_{el} is the electrical efficiency of the module as a function of G and T, T_{mod} is the temperature of the PVT module, G_{ref} is the reference irradiation, set to 1000 W/m^2, T_{ref} is the reference module temperature set to 25 °C, and β is the temperature coefficient of MPP power.

During periods when solar irradiance is insufficient to raise the circulating water temperature above that of the water tank, the loop is closed to prevent the tank from cooling. The collector temperature is no longer determined by water temperature but instead influenced by other, less significant factors. To determine the module temperature in this case, which is essential for calculating electrical and thermal efficiency, a new energy balance is considered. This balance takes into account the solar thermal energy absorbed by the panels, the convective heat transfer with the air above the panels, and thermal energy radiation, and is represented by Eq. (5) [27]:

$$M_{\mathrm{PV}} c_{\mathrm{p,PV}} \frac{dT_{\mathrm{mod}}}{dt} = A_{\mathrm{PVT}}(\alpha G(1-\eta_{\mathrm{el,ref}}) - h_{\mathrm{conv}}(T_{\mathrm{mod}} - T_{\mathrm{a}}) - \sigma\varepsilon(T_{\mathrm{mod}}^4 - T_{\mathrm{sky}}^4)), \tag{5}$$

where M_{PV} is the mass of PV cells in the PVT module, $c_{\mathrm{p,PV}}$, is the thermal capacity of the PV cells in PVT module, A_{PVT}, is the module aperture area, α is the absorptivity, $\eta_{\mathrm{el,ref}}$ is the electrical efficiency of reference, h_{conv} is the convective heat transfer coefficient between the PVT module and the surrounding air, σ is the Stefan–Boltzmann constant, ε is the emissivity, and T_{sky} is the representative temperature of the sky.

Several studies have based their PVT collector models on real manufacturer data, frequently referencing the company Endef Solar Solution for this purpose. Their Ecomesh model, showing high thermal efficiency, particularly important in colder climates such as Germany, is selected. The selection of the Ecomesh is also supported by its use in previous studies with similar objectives, increasing its compatibility with existing research [28–32]. The characteristics for the Ecomesh are summarized in Table 1.

Table 1
PVT system parameters.

Category	Parameter	Ecomesh	Unit
General	Type	flat plate cov.	–
	Price	494	Euro
	Aperture area	1.55	m^2
	Mass flow rate	50	kg/h c
Electrical	Electrical eff. (ref)	16.0	%
	Temp. coef. (β)	$-4.70 \cdot 10^{-3}$	1/K
	Reference temp.	298	K
	Nominal power output	260	W
Thermal	Optical eff.	51.0	%
	1st-order heat loss coef.	4.93	W/m^2 K
	2nd-order heat loss coef.	0.04	W/m^2 K^2

2.1.2. Heat pump

The HP cycle is a basic four-component refrigerant cycle, with an evaporator, a compressor, a condenser, and an electronic expansion valve. The assumed HP possesses a variable-speed compressor and a control system able to provide part-load heating from half of the design output and upwards depending on the working conditions. Moreover, just as for most recent HP models, a small electrical immersion heater is assumed to be integrated in the HP design to compensate for hours of high heating demand. The HP is governed by a control system surrounding two conditions:

1. Maintaining the tank temperature above 50 °C.
2. Making use of the excess solar electricity remaining after covering all the electricity demand for the appliances and lighting.

The first condition has priority over the second and the control of the HP varies between an on–off system for condition 1 and a variable heat output for condition 2. Eq. (6) summarizes the conditions by giving the instantaneous HP heat output:

$$\dot{Q}_{\mathrm{HP}} = \begin{cases} \dot{Q}_{\max}, & \text{if } T_{\mathrm{WT}} \le T_{\min} \\ f(P_{\mathrm{exc,app}}), & \text{if } P_{\mathrm{exc,app}} \ge P_{\mathrm{exc,lim}} \& T_{\min} < T_{\mathrm{WT}} < T_{\max} \\ 0, & \text{if } P_{\mathrm{exc,app}} < P_{\mathrm{exc,lim}} \& T_{\mathrm{WT}} > T_{\min}, \end{cases} \tag{6}$$

where $\dot{Q}_{\mathrm{HP}}$ is the heat output from the HP, $\dot{Q}_{\max}$ is the design heat output from the HP, T_{WT} is the water tank temperature, $T_{\min}$ is the limit temperature, set to 55 °C, above which the HP is activated at full power, $T_{\max}$ is the limit temperature, set to 65 °C, above which the HP is not activated even if the excess electricity is abundant, $P_{\mathrm{exc,app}}$ is the excess solar electrical power after use from appliances and lighting, and $P_{\mathrm{exc,lim}}$ is the limit on $P_{\mathrm{exc,app}}$ above which the HP is activated as a function of $P_{\mathrm{exc,app}}$. The variable heat output function, denoted as f, which correlates with the surplus electricity after fulfilling the requirements of appliances and lighting, varies based on the quantity of this surplus. Its formulation is described in Eq. (7):

$$f(P_{\mathrm{exc,app}}) = \begin{cases} \dot{Q}_{\max}/2, & \text{if } P_{\mathrm{exc,app}} < \dot{Q}_{\max}/(2 \cdot \mathrm{COP}) \\ P_{\mathrm{exc,app}} \cdot COP & \text{if } \dot{Q}_{\max}/(2 \cdot \mathrm{COP}) \le P_{\mathrm{exc,app}} \le \dot{Q}_{\max}/\mathrm{COP} \\ \dot{Q}_{\max} & \text{if } P_{\mathrm{exc,app}} > \dot{Q}_{\max}/\mathrm{COP}, \end{cases} \tag{7}$$

where COP represents the HP coefficient of performance. $P_{\mathrm{exc,lim}}$ is set to half the minimum part load, i.e. one fourth of the design heat output. The motivation for this choice, is to maximize the use of solar electrical power. It is more advantageous to pre-charge the water tank using up to 50% grid electricity and the remainder from PV-sourced electricity, rather than relying predominantly on grid electricity for immediate heating needs.

The electrical heater is activated only to boost the tank temperature if the HP is insufficient, which only happens infrequently. Its thermal output is regulated by an on–off control and its COP is assumed to be equal to 1.

This study aims to test the SAHP for a wide variety of HP designs, obtained through a separate technoeconomic HP design model

Table 2
Design parameters and mean COP in off-design for the 9 selected designs. The reference design is highlighted in gray.

Design	Heat output (W)	PPTD (°C)	Total cost (Euro)	Refrigerant	Design temp. (°C)	Mean COP
High performing	5500	3	4976.6	R32	−6.1	3.12
	5500	3	5021.0	R410a	−6.1	2.93
	5500	3	5300.3	Propane	−6.1	3.11
Medium performing	5500	5	4931.1	R32	−6.1	2.86
	5500	5	4868.6	R410a	−8.3	2.2
	5500	5	5122.1	Propane	−6.1	2.85
Low performing	5500	10	4783.6	R32	−6.1	2.47
	5500	10	4711.9	R410a	−6.1	2.0
	5500	10	4977.9	Propane	−6.1	2.28

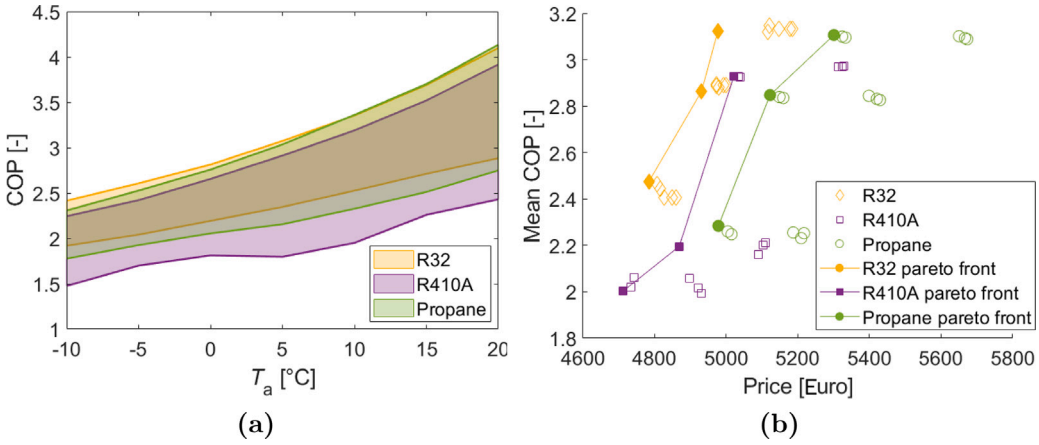

Fig. 2. Plots including 18 designs for each refrigerant depicting: (a) the range of COP/temperature correlation, (b) the mean COP in off-design and the costs off all HP designs, specifying the designs selected for further investigation.

developed internally partially by the authors, prioritizing different characteristics such as thermodynamic performance, costs and environmental impact [33]. The design of each HP is based on the following input parameters: cold-source temperature, hot-sink temperature, heat output, refrigerant, compressor type, and the pinch-point temperature difference (PPTD), defined as the smallest temperature difference between brine and the working fluid in the HEXs. A range of values is tested for most design parameters, with the motivation explained in Appendix B. The combination of all different parameters yield 54 designs summarized in Table B.1.

The HP model is a detailed thermodynamic model that provides optimized estimates of COP as a function of Ta, assuming a fixed hot-sink temperature. Exponential regression fits are obtained from these estimates and are used as input to the SAHP model. A range of COP/temperature correlations containing 18 designs for each refrigerant are depicted in Fig. 2(a), while the mean COP values are illustrated in Fig. 2(b). For each refrigerant three designs were selected:

1. A high-performing, more costly design, corresponding to the one with the highest mean COP, without compromising too much for cost.
2. A low-cost, lower-performing design, corresponding to the one with the lowest total cost.
3. A medium performing design, corresponding to the one offering an average COP for a reasonable price.

The 9 selected designs are summarized in Table 2 and Fig. 2(b). Given its prevalence in newly installed HPs, the R32 refrigerant is the most widespread choice. Therefore, among the nine selected designs, the medium performance R32 variant was chosen as the reference design for generating results in Section 3.

2.1.3. Water storage tank

The thermal energy demand does not always coincide with the thermal energy production, and the tank serves as thermal energy storage to compensate for the mismatch. Given the use of a one-node (fully mixed) tank model, a relatively large storage volume was required to meet system constraints, particularly the minimum hot water temperature [34–36]. A 750 L tank by the manufacturer RVR Energy Technology was chosen as reference for the thermal tank [37]. The water storage tank energy balance constitutes the main equation of the SAHP system. It relates the energy inputs to, and the outputs from, the tank to the change in the stored tank energy, as depicted in Eq. (8):

$$M_{\mathrm{WT}} c_{\mathrm{p,water}} \frac{dT_{\mathrm{WT}}}{dt} = \eta_{HEX}\dot{Q}_{\mathrm{HP}} + \dot{Q}_{\mathrm{PVT}} - \dot{Q}_{\mathrm{SH}} - \dot{Q}_{\mathrm{HW}} - \dot{Q}_{\mathrm{losses}} + \dot{Q}_{\mathrm{aux}}, \quad (8)$$

where M_{WT} is the total mass of water in the storage tank, $c_{\mathrm{p,water}}$ is the specific heat capacity of water, η_{HEX} is the HEX efficiency, set to 0.9, $\dot{Q}_{\mathrm{SH}}$ is the heat flow from the water tank to the space heating water, $\dot{Q}_{\mathrm{HW}}$ is the heat flow from the water tank to the domestic hot water, $\dot{Q}_{\mathrm{losses}}$ is the heat flow between the water storage tank and the environment, and $\dot{Q}_{\mathrm{aux}}$ is the heat flow from the auxiliary electrical heater to the water tank.

The differential Eq. (8) is solved for T_{WT} and the temperatures at the inlet and outlet of the PVT collectors using the backward Euler method on an hourly time scale. The main assumptions required for the numerical resolution are threefold [29]:

1. Perfect mixing: there are no spatial gradients in the physical envelope of the water inside the tank.
2. The total mass of the tank is constant.
3. The specific heat capacity is assumed to be constant in the relevant temperature range.

Replacing the one-node model by a vertically stratified tank model could improve storage efficiency and reduce the necessary tank size. This is recommended for future work but left outside of the scope of this study.

Losses through the tank are the only losses accounted for in the SAHP model. Other losses are assumed to be negligible due to the shorter retention times and smaller HTF volumes in the other components compared to the water tank. The surface area and the insulation thickness are used to determine the losses through the tank insulation to the surrounding air using Eq. (9) [38]:

$$\dot{Q}_{\text{losses}} = A_{\text{WT}} U_{\text{ins}} (T_{\text{a}} - T_{\text{WT}}), \tag{9}$$

where A_{WT} is the external surface area of the water tank, U_{ins} is the overall heat-transfer coefficient that accounts for heat losses from the tank to the ambient air see Appendix A.

2.2. Economic and environmental indicators

In addition to assessing thermodynamic performance, this study analyzes economic and environmental indicators [29,39–41]. The cost savings (CS) in comparison to a natural gas boiler heating system are determined by subtracting the operating costs of the SAHP system from those of the boiler system, and adding the revenues from excess electricity production as in Eq. (10):

$$CS = C_{\text{O\&M,boiler}} - C_{\text{O\&M,SAHP}} + (E_{\text{app,cov}} - E_{\text{HP,uncov}}) c_{\text{e}} + \frac{(Q_{\text{HW}} + Q_{\text{SH}})}{\eta_{\text{boiler}}} c_{\text{ng}} + E_{\text{exc}} s_{\text{e}}, \tag{10}$$

where $C_{\text{O\&M,boiler}}$ and $C_{\text{O\&M,SAHP}}$ are the costs of operation and maintenance for the boiler and the SAHP respectively, c_{e} is the cost of electricity, s_{e} is the selling price of electricity, determined from the German feed-in-tariff system, $E_{\text{app,cov}}$ is the electricity demand of appliances and lighting covered by the solar-sourced electricity, $E_{\text{HP,uncov}}$ is the electricity demand of HP not covered by solar-sourced electricity, Q_{SH} and Q_{HW} are the SHD and HWD respectively, covered by the SAHP, and E_{exc} is the electricity sold to the grid. The net present value (NPV) is calculated with Eq. (11):

$$NPV = -I_{\text{o}} + \frac{CS}{d - i_{\text{f}}} \left(1 - \left(\frac{1 + i_{\text{f}}}{1 + d}\right)^{n}\right), \tag{11}$$

where I_{o} is the initial investment, including PVT array, HP, water storage tank, HTF, mounting costs, installation costs, piping, pump station, controller, expansion vessel, d is the discount rate, i_{f} is the inflation rate, n is the investment horizon considered, set to 20 years. The payback time (PBT) is obtained with Eq. (12):

$$PBT = \frac{ln\left(\frac{I_{\text{o}}(i_{\text{f}} - d)}{CS} + 1\right)}{ln\left(\frac{1 + i_{\text{f}}}{1 + d}\right)} \tag{12}$$

The levelized cost of energy in electricity equivalents ($LCOE_{\text{eq,el}}$) evaluates the total costs per energy unit associated with the actual electrical and thermal energy output. The thermal output is assumed equivalent to the electricity which could have been produced from that heat in a natural gas power plant. The $LCOE_{\text{eq,el}}$ is calculated using Eq. (13) [42]:

$$LCOE_{\text{eq,el}} = \frac{I_{\text{o}} + \sum_{i=1}^{n} C_{\text{prod}} (1 + i_{\text{f}})^{i-1} (1 + d)^{-i}}{\sum_{i=1}^{n} (Q_{\text{el}} + Q_{\text{th}} \eta_{\text{th}}) (1 + d)^{-i}}, \tag{13}$$

where C_{prod} are the yearly costs related to energy production, Q_{el} is the net annual production of electricity, Q_{th} is the net annual production of heat, η_{th} is the typical efficiency of a modern natural gas power plant, from thermal to electrical, set to 55%. Moreover, emission reduction (ER) is determined to estimate the environmental penalty cost savings ($EPCS$) see Eqs. (14) and (15):

$$ER = (E_{\text{exc}} + E_{\text{app,cov}} - E_{\text{HP,uncov}}) f_{\text{el}} + \frac{(Q_{\text{SH}} + Q_{\text{HW}}) f_{\text{ng}}}{\eta_{\text{boiler}}}, \tag{14}$$

$$EPCS = \frac{ER\, C_{CO_2}}{d - i_{\text{f}}} \left(1 - \left(\frac{1 + i_{\text{f}}}{1 + d}\right)^{n}\right), \tag{15}$$

where f_{el} is the CO_2 emission factor of electricity, f_{ng} is the CO_2 emission factor of natural gas, C_{CO_2} is the cost of unit emission of CO_2, according to the EU emission trading system (ETS). Despite the absence of environmental penalty costs in the residential sector presently, future carbon pricing initiatives are expected, explaining why the unit cost of CO_2 emissions was considered in Eq. (15) [42–44]. CS and $EPCS$ were summed to determine the total cost savings (TCS).

2.3. Data acquisition

2.3.1. Thermal energy demand

In this study thermal energy demand is described in terms of useful energy demand, representing the net energy required to satisfy SHD or HWD [45]. Model input parameters include the annual SHD and HWD of a typical SFH and its normalized hourly heat demand load profile. The annual SHD and HWD is obtained from the EUs Moderate project, which offers comprehensive data on the European building stock across different building types, including SFHs [45]. The heating demand profiles for Germany in the year 2020 are obtained from the When2heat database, providing country specific normalized profiles for the EU28 [46].

Typical winter and summer week profiles are selected for further analysis and are provided in Fig. 3. Weeks with the closest match to the average weekly heat demand for each season are used as representative periods. Data aggregated by month is summarized in Fig. 4.

2.3.2. Electricity demand

To incorporate electricity demand into the model, both the electricity load profile and the total yearly electricity load for appliances excluding any electricity used for heating purposes are necessary. Data on final energy consumption for lighting and electrical appliances in the residential sector, sourced from Eurostat, are employed for the total load [47]. Developing a load profile specifically adapted to SFHs or the residential sector also excluding electricity used for heating was deemed overly precise. Instead, the actual total hourly load for Germany for 2020, obtained from the Entsoe Transparency Platform, is utilized to derive a normalized load profile. Data aggregated by month is summarized in Fig. 4.

2.3.3. Weather data

The SAHP model requires hourly temperature, irradiation, and wind speed profiles to predict the behavior of the PVT collectors, the HP, and the water tank. Data from 2020 for the three studied cities were sought. The PVGIS-SARAH2 tool from the European commission provided the researched figures, given as 2-m air temperature, global irradiance on the plane of the array and 10-m total wind speed [48].

Test simulations revealed that heat demand coverage by solar energy for the reference SAHP in Munich reached around 38% while it only reached 35% in Berlin and 31% in Hamburg. As a result, weather data from Munich was selected for subsequent analysis.

2.3.4. House specifications

House-specific parameters provided as model input are reported in Table 3 [45]. To translate the constructed floor area of the house to the rooftop area, the average amount of floors and average roof slope was used [49]. Additionally, to convert the rooftop area into usable area for PVT arrays, an average rooftop utilization factor is employed.

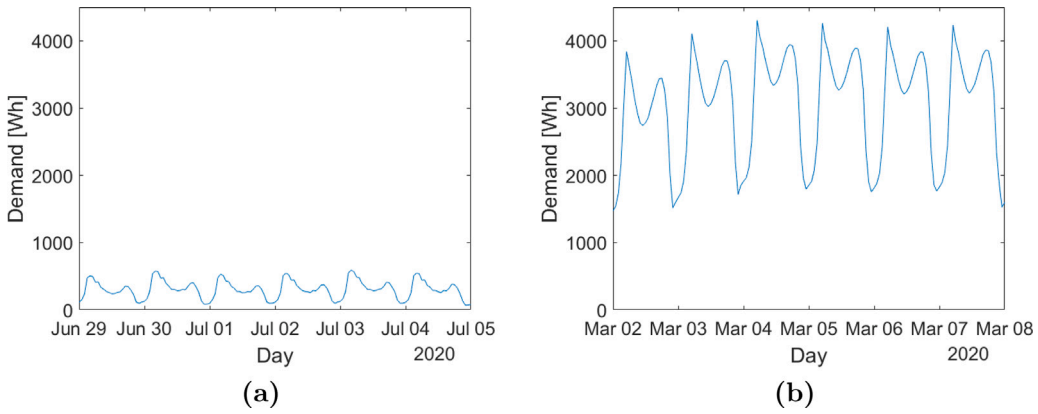

Fig. 3. SFH total heat demand for the average week: (a) summer, and (b) winter.

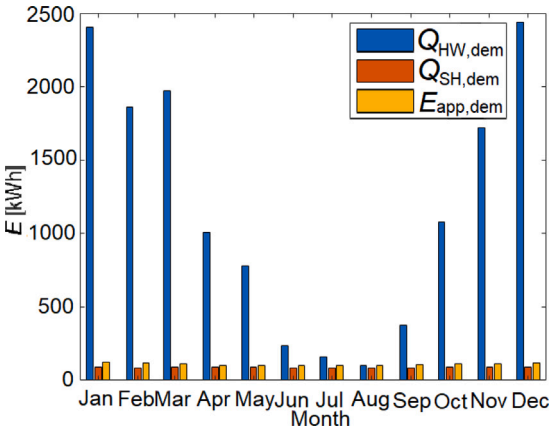

Fig. 4. Thermal and electrical energy demand by month.

Table 3
House specifications.

Specification	Value	Unit
Heated floor area	89.1	m^2
Floor area	93.1	m^2
Roof area	82.4	m^2
Rooftop utilization factor	0.4	ratio
Area covered by PVT	32.9	m^2

Table 4
Investment costs for the systems.

System	Component	Value	Unit
PVT system	PVT collector	1.9 [28]	Euro/W
	Expansion vessel	140 [29]	Euro/set
	Pipes	11 [42]	Euro/m
	HTF	3.3 [42]	Euro/L
	Mounting	59 [42]	Euro/collector
	Installation	40 [42]	Euro/m^2
	$C_{O\&M}$	0.01 C_0 [42]	Euro/year
	Controller	110 [29]	Euro
	Inverter	0.2 [28]	Euro/W
HP system	C_0	$4712 < C_0 < 5673$	Euro
	Installation	2529 [50]	Euro
	$C_{O\&M}$	115 [50]	Euro
Water storage tank	C_0	$0.874 \cdot V_t$ (L) + 763.5 [29]	Euro
Standalone boiler	C_0	1724 [51]	Euro
	Installation	2625 [51]	Euro
	$C_{O\&M}$	115 [52]	Euro/year

Table 5
Economic parameters.

Variable	Value	Unit
Exchange rate	1.1495 [53]	Euro/pound
Electricity purchase price	0.2333 [54]	Euro/kWh
Electricity selling price	0.086 [55]	Euro/kWh
Natural gas price	0.093 [56]	Euro/kWh
Interannual inflation rate	0.0459 [57]	Rate
Discount rate	0.0366 [58]	Rate
SAHP lifetime	20 [59]	Years
HP lifetime	20 [59]	Years
Boiler lifetime	14 [60]	Years
Emission factor of electricity	0.381 [61]	$kgCO_2$/kWh
Emission factor of natural gas	0.20099 [62]	$kgCO_2$/kWh
Cost of unit CO_2 emission	0.084 [63]	Euro/$kgCO_2$

2.3.5. Economical and environmental parameters

C_0 and $C_{O\&M}$ for the components of the studied systems are summarized in Table 4. C_0 for the HP designs are given by the HP model and include the auxiliary electrical heater. These figures are applicable to HP systems within the size range of 3 to 10 kWth. For the PVT systems, which are neither excessively small nor large, the provided figures are reasonable within their size range. Values given per unit of power, W, refer to the nominal electrical power. Parameters relevant for all studied system are summarized in Table 5. Instead of selecting values from the same reference year as for the energy demand and load profiles, prioritizing recent data was considered more crucial, given the aim of assessing the future potential of SAHPs. Typically, values are reported annually, and the most recent ones available are selected.

3. Results and discussion

3.1. Hourly transient operation

This section provides results from the transient SAHP model for different scales, showcasing different trends. The focus is not on comparing different HP designs. Therefore, only the reference design and weather data for Munich are utilized for this section.

3.1.1. Temperature-dependent parameters

The annual profiles for T_a, T_{WT}, and T_{PVT} (the temperature of the water exiting the PVT collectors is considered) are shown on an hourly resolution in Fig. 5.

T_{PVT} is influenced by the circulating water only during periods of high irradiance and temperature when the loop is open. When the loop is closed, T_{PVT} is affected by T_a and wind conditions. This results in the rapid temperature variation for T_{PVT} compared to T_{WT} and T_a, observed both on a daily and seasonal basis. Indeed, during the day, specifically during summer, the increased T_a and solar irradiance make it more likely for the solar loop to be open. The opposite is true during the night

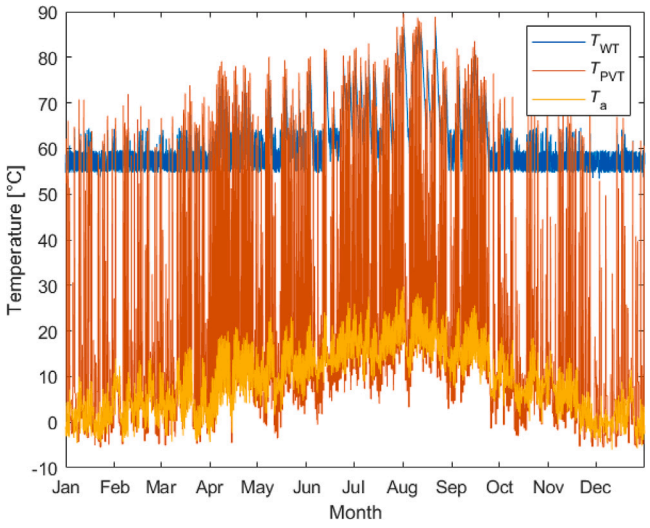

Fig. 5. Water tank temperature profile (T_{WT}), PVT outlet temperature (T_{PVT}) and ambient temperature profile (T_a), provided with hourly scale.

and during winter and T_{PVT} occasionally drops below 0 °C. The risk of freezing is discussed in Section 5, defrosting for IDX SAHPs should be included in future modeling work.

T_{WT} is successfully maintained above 55 °C for the majority of the modeled hours. T_{WT} never dips below 50 °C, as the tank is large enough to prevent such dips, with assistance from the auxiliary heater. Noteworthy, is that the auxiliary heater remains inactive for almost the entire year, only engaging for a few hours intermittently during the winter. T_{WT} only exceeds the upper HP temperature limit of 65 °C when the solar loop is open, and the PVT collectors heat the tank instead of the HP.

The electrical and thermal efficiency of the PVT collector, and the HP COP, are influenced by the temperature profiles and are depicted in Fig. 6:

When irradiance is zero, the electrical efficiency of the PVT module drops to zero. Similarly, the thermal efficiency of the PVT collectors is zero when the temperature within the collectors is too low. Due to diurnal fluctuations in electrical and thermal efficiencies, the maximum daily efficiencies are plotted instead of hourly efficiency values to enhance readability and comparability.

Regarding electrical efficiency, η_{el}, shown in Fig. 6(a), it never reaches zero since some daily solar irradiance always persists throughout the year. According to Eq. (4), η_{el} increases as T_{mod} decreases. One advantage of the PVT collectors is that the temperature of the PVT collectors decreases because the circulating water absorbs heat. However, η_{el} decreases in the summer. Meaning that the increase in ambient temperature during the summer leads to a rise in T_{mod}, which the heat absorption by the collectors cannot fully compensate for. A suggestion for future modeling work, left beyond the scope of this study, is the inclusion of an air heater to dissipate excess heat and reduce T_{mod} during the summer.

The thermal efficiency, η_{th}, plotted in Fig. 6(b), remains at zero for many days of the year, especially in winter, due to insufficient temperature and irradiance levels to open the solar loop, resulting in no solar thermal energy transfer to the tank. When the solar loop is open, η_{th} decreases with increasing T_a and irradiance but increases with a higher T_{MF}, according to Eq. (1). T_{MF} is in its turn determined by T_{WT} and is kept above 55 °C, explaining the much smaller η_{th} in comparison to the reference optical efficiency in Table 1. As η_{th} increases during the summer months, as shown in Fig. 6(b), it suggests that the rise in ambient temperature and irradiance outweighs the increase in T_{MF}.

Finally, the COP of a HP increases when the temperature difference between the hot sink and the cold source decreases. Since T_{WT} varies by no more than 10 °C when the HP is activated, the COP is primarily influenced by T_a. Coherently, the peak COP, shown in Fig. 6(c), occurs at the warmest point of the year in September.

3.1.2. Typical week profiles

Demand coverage is plotted in Fig. 8 for heat and in Fig. 9 for electricity. In Fig. 8, thermal energy supplied to the tank is split into solar thermal or HP input. The HP input is further divide based on the electricity used, grid or solar-sourced. Fig. 9 distinguishes between grid and solar-sourced electricity not only for the HP but also for the rest of the appliances. Excess electricity is also considered. Consistent parameters and descriptive legends are used throughout the plotted results in this paper. To explain the parameters and legends in Figs. 8, 9, and subsequent figures, flow diagrams are presented in Fig. 7.

A common trend in all the figures is the daily peaks in solar energy production, corresponding to the hours of peak irradiance. Specifically, Fig. 8(a) shows that the irradiance peak corresponds to a peak in PVT, th; Fig. 8(b) shows a peak in $HP\ PVT, el$; Fig. 9(a) shows a peak in exc; and Fig. 9(b) shows a peak in $HP\ PVT$.

During a typical summer week, observed in Figs. 8(a) and 9(a), most of the low heating demand is met by the thermal output of the PVT collectors, meaning that less solar electricity is used by the HP and more is used by the rest of the appliances. This leads to a large demand coverage by solar for the rest of the appliances as well as large excess electricity generation, as shown in Figs. 8(a) and 9(a). The HP cannot run on either solar or grid electricity because the water tank is already charged to a high temperature, exceeding the 65 °C limit, most of the week.

On the contrary, during a typical winter week, observed in Figs. 8(a) and 9(a), the HP is running on full load (5500 W) frequently throughout the week. However, the unfavorable weather conditions hinder the effective operation of the PVT solar loop, and solar energy is instead occasionally used by the HP in the form of electricity. Only a small portion of the large heating demand is met by solar energy, as seen in Fig. 8(b). However, when it comes to electricity use around half of the demand from the rest of the appliances can still be covered, but minimal excess electricity is produced, as shown in Fig. 9(b).

3.1.3. Monthly aggregation

Aggregating the results on a monthly scale provides a clearer understanding of demand coverage throughout the year. The heat demand coverage and electricity use are illustrated in Figs. 10 and 11, following the legend description from Fig. 7.

When it comes to the heat input plot in Fig. 10, the coverage by solar energy is more substantial during the summer months. In July and August, nearly all heat demand is met by solar sourced energy, specifically by the solar thermal input (PVT, th). From April to September, the majority of the heat input to the tank originates from solar energy, both as solar thermal input and as input from the HP running on solar-sourced electricity ($HP\ PVT, el$). During the autumn and winter months, the months with the highest heat demand, the heat input to the tank primarily comes from the HP operating on grid electricity. Indeed, η_{th} is generally lower during the autumn and winter, oftentimes zero, when the solar loop is closed, as observed in Fig. 6(b). T_{MF} is too high to ensure continuous efficient solar thermal provision throughout the year, and future research on the topic of emerging heating systems with low temperature thermal storage such as fan coils or floor heating would be of relevance to address this issue.

Over the course of the year, the HP powered by solar electricity generally contributes more than the solar thermal input, with the exception of July and August. This deviation is due to the HP's control system: during these months. As the PVT collectors generate thermal energy and the tank temperature exceeds the HP's upper limit of 65 °C, the HP can no longer use solar electricity for charging. The HP's ability

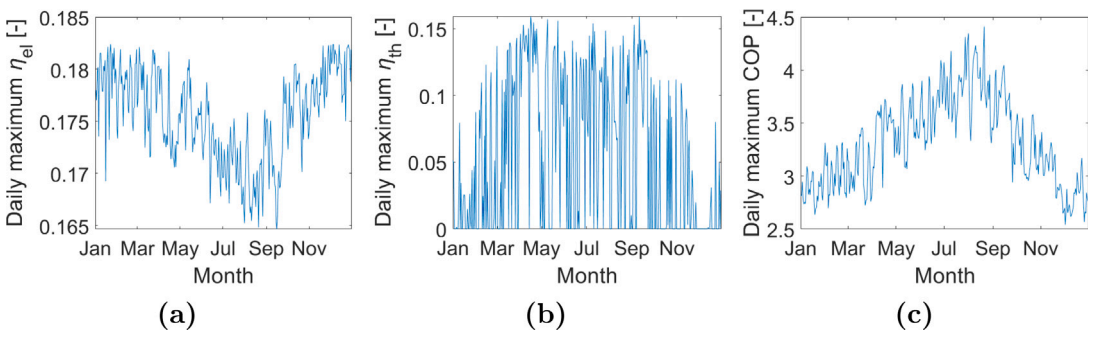

Fig. 6. Efficiency metrics on hourly scale: (a) PVT electrical efficiency, (b) PVT thermal efficiency, and (c) HP COP.

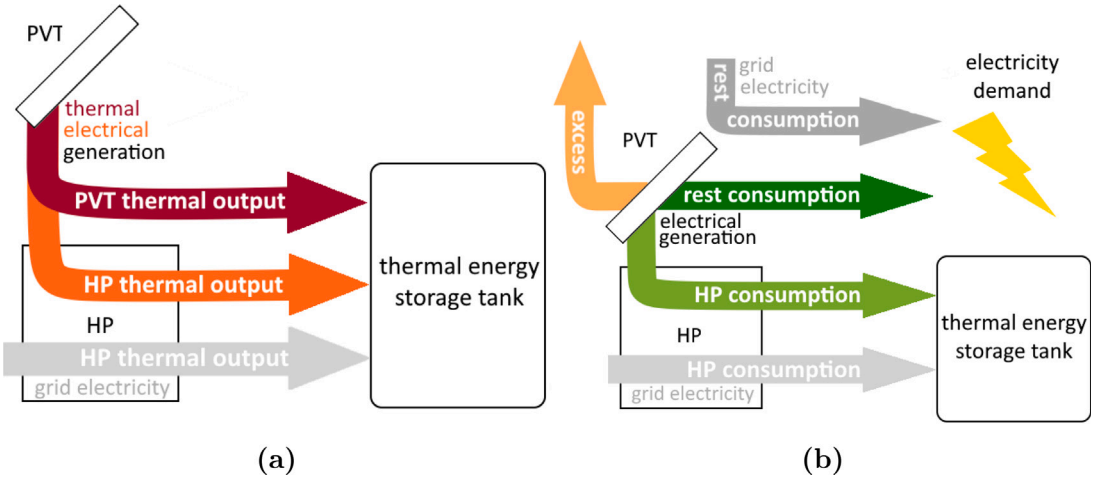

Fig. 7. Flow diagram, color-coded to subsequent figures, describing: (a) heat inputs to the tank, and (b) electricity use.

to operate on solar-generated electricity diminishes as the SAHP gains the ability to extract solar thermal output. Suggestions avoiding this issue are: changing the HP control system to allow HP output further surpassing the design output temperature, dividing the heat output from the HP and the PVT solar loop into two different water tanks, or using a serial instead of a parallel SAHP configuration.

In the electricity plots in Fig. 11, the bottom three bars represent the division of generated electricity, indicated by the yellow dotted line, into usage by the HP, usage by the rest of the appliances, and excess electricity. The two bars above these illustrate the division of grid electricity usage into usage by the HP and usage by the rest of the appliances. The pink dotted line represents the electricity demand.

For the same reasons as described for Fig. 10, the solar electricity consumed by the HP ($HP\ PVT$) decreases in summer and increases in winter, as shown in Fig. 11. Meanwhile, the consumption by other appliances ($rest\ PVT$) follows the opposite trend. Unlike the heat demand, the electricity demand of other appliances remains relatively constant throughout the year. This steady demand, combined with increased solar electricity in summer, results in the higher solar coverage for other appliances during this time.

Throughout the year, a significant amount of excess electricity is generated. In the summer, the high excess electricity is due to the low demand. In the colder months, the excess electricity arises from the mismatch between the times of electricity generation and consumption. The seasonal demand difference and the mismatch between generated and consumed electricity also explain why the grid electricity consumption, for both the HP and other appliances, is minimal in the summer and significantly higher in the remaining months.

3.2. Annual comparison of different heat pumps

The nine selected HP designs are compared thermodynamically, economically and environmentally in the SAHP context. The thermodynamic comparison was performed by examining the yearly aggregated demand coverage for both thermal and electrical energy in Figs. 12 and 13, following the legend description from Fig. 7. The economic and environmental comparison was conducted by evaluating key parameters summarized in Table 6. These simulations were based on weather data from Munich.

Firstly, in Fig. 12, the top of the bars reach the same height for all designs because the water tank requires the same thermal input regardless of the design. The solar thermal input to the tank (PVT, th) also remains mainly constant regardless of HP design because the performance of the PVT collectors is largely independent of the HP's performance. The heat input to the tank, the HP input ($HP\ PVT, el$ and $HP\ grid$) is the relevant part depicted in Fig. 12.

A clear trend emerges: looking at each refrigerant individually, enhanced performance correlates with an increased proportion of HP output derived from solar electrical energy ($HP\ PVT, el$). The higher COP values related to the increase in performance means that the solar-sourced electricity can be used to produce a larger HP output, explaining the trend.

Additionally, a consistent ranking among the refrigerants is evident. The R32 design exhibits higher solar coverage compared to the propane design, which in turn shows higher coverage than the R410 A design, across all performance levels studied. R32 and propane have comparable solar coverage, reaching up to 39% for the high-performing designs, while R410 A shows a significantly lower coverage. This is explained by the higher COP values found for R32 and propane designs as seen in Fig. 2(a).

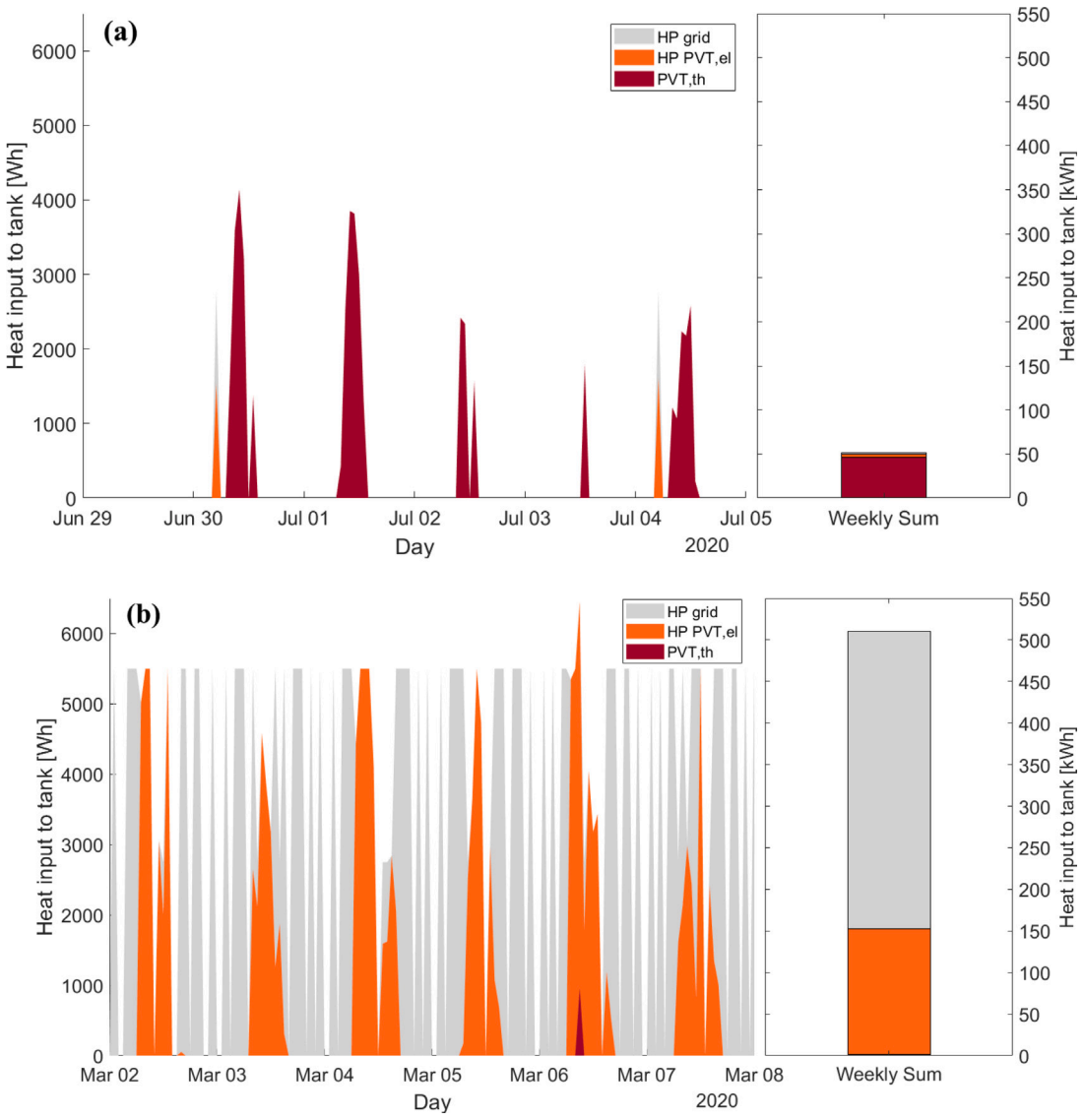

Fig. 8. Heat demand coverage of the SAHP during: (a) the average summer week, and (b) the average winter week; depicting solar thermal energy (PVT, th), HP input when run on solar-sourced electricity ($HP\ PVT, el$), and when run on grid electricity ($HP\ grid$).

Secondly, in analyzing the electricity use depicted in Fig. 13, differences in the COP for each HP design result in varying amounts of electrical energy needed to cover the thermal input to the tank, leading to the differing bar sizes, in contrast to Fig. 12. The three lower bars represent generated electricity, with the top of the third bar (exc) reaching the same amount for each HP design. This is expected since solar electrical generation depends on the PVT collector electrical performance, which remains largely unaffected by HP performance. The consumption of the rest of the appliances ($rest\ PVT$ and $rest\ grid$) also remains unaffected by HP design since the solar electricity covers the appliances before covering the HP demand.

The light green ($HP\ PVT$) and light gray ($HP\ grid$) bars, which together correspond to the total HP electricity consumption show that improved HP design performance results in decreased energy consumption by the HP, observable for each refrigerant. This reduction in energy consumption, again, aligns with the increase in COP, used as a proxy for performance level characterization.

Additionally, the electricity use plot reveals the same refrigerant ranking mentioned earlier. The R410 A design consumes significantly more electricity than the other two designs, by up to a couple of thousand kWh. The R32 and propane designs exhibit similar electricity consumption, with the R32 design slightly outperforming the propane design.

Analyzing Table 6, reveals several key trends. The first column, showing the C_0, indicates a price increase with enhanced HP performance for each refrigerant. This rise is primarily due to the decrease in PPTD and the corresponding increase in HEX sizes. Propane designs exhibit higher investment costs compared to R32 and R410 A designs, which display similar price levels at each performance tier. The subsequent columns reveal two overarching trends:

Firstly, higher HP performance levels correlate with better economic and environmental metrics for each refrigerant individually. As HP performance improves, the $LCOE_{\text{eqel}}$ and PBT decrease, CS, NPV, ER, $EPCS$, and TCS increase. The advantage of higher solar coverage in high-performing HP designs, observed in the previous figures, reduces the reliance on grid electricity, resulting in both financial and environmental benefits. This advantage outweighs the higher C_0 associated with high-performing HP designs.

Secondly, R32 designs exhibit superior economic and environmental performance compared to propane designs, which in turn outperform R410 A designs at each performance level. This ranking pattern is consistent with previous observations on solar coverage and can again

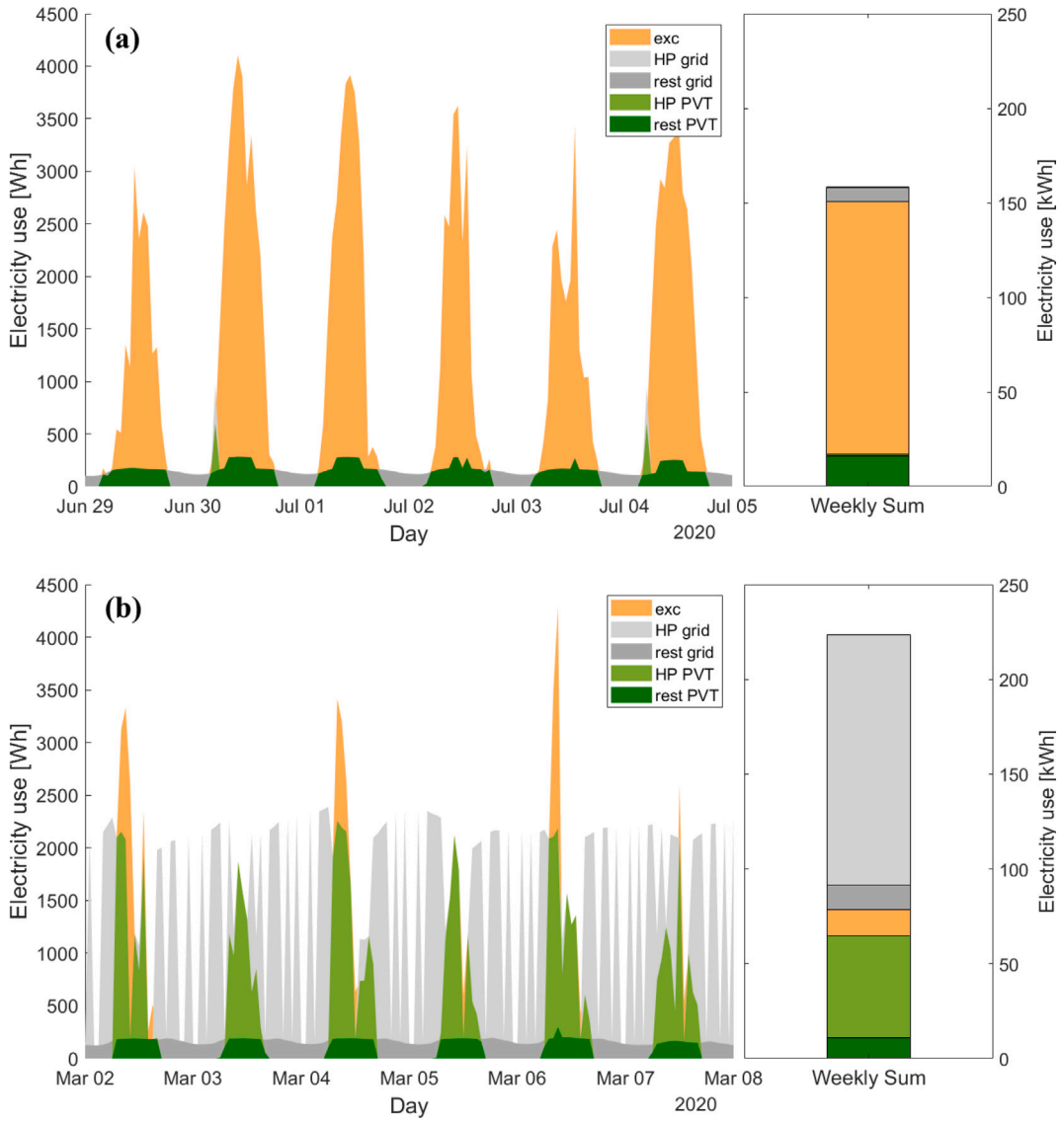

Fig. 9. Electricity use during: (a) the average summer week, and (b) the average winter week; depicting solar-sourced electricity going to the appliances (*rest PVT*), and to the HP (*HP PVT*), as well as the excess (*exc*), the grid electricity used for the appliances (*rest grid*), and for the HP (*HP grid*).

Table 6
Economical and environmental metrics for the SAHP system for different HP designs.

Perf.	Design	C_0 (Euro)	$LCOE_{eq,el}$ (Euro/kWh)	CS (Euro)	PBT (years)	NPV (Euro)	ER ($kgCO_2$)	$EPCS$ (Euro)	TCS (Euro)
High	R32	22 856	0.272	1133	19.3	960	4396	7766	8898
	R410A	22 901	0.283	1038	20.9	−1076	4252	7512	8550
	Propane	23 180	0.276	1114	19.8	255	4370	7720	8834
Med	R32	22 811	0.285	1012	21.3	−1519	4213	7443	8455
	R410A	22 749	0.340	537	37.2	−11459	3499	6182	6718
	Propane	23 002	0.288	1000	21.7	−1982	4194	7409	8409
Low	R32	22 664	0.309	797	26.3	−5905	3880	6855	7652
	R410A	22 592	0.354	407	46.6	−14027	3306	5840	6248
	Propane	22 858	0.325	671	30.8	−8748	3689	6517	7188

be explained by differences in COP values. It is noteworthy that the higher C_0 of propane designs do not prevent them from achieving better values than R410 A designs, despite the latter having investment costs closer to those of R32 designs.

Additionally, it is important to note that the high-performing R32 and propane designs are the only ones with a positive NPV and a PBT lower than their 20-year project lifetimes, making them the only financially viable investments among those tested.

Observing that R32 and propane outperform R410 A in previous results is positive, as R410 A has the highest global warming potential (GWP) among them. From an environmental perspective, R32 and propane are preferable choices, providing another reason to exclude R410 A in future SAHPs. Propane, with a lower GWP than R32 and an ozone depletion potential of 0, could be the refrigerant of the future. However, it is important to consider the high flammability of propane and the associated safety risks. Considering carbon taxation and the

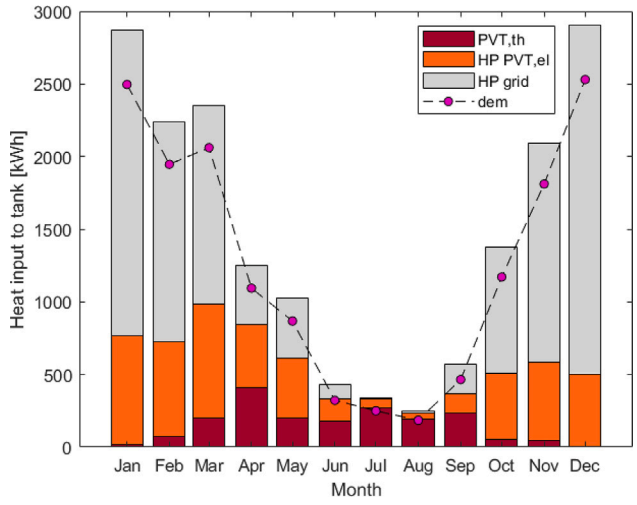

Fig. 10. Heat demand coverage of the SAHP on monthly scale, depicting heat demand (dem), solar thermal energy (PVT,th), HP input when run on solar-sourced electricity ($HP\ PVT,el$), and when run on grid electricity ($HP\ grid$).

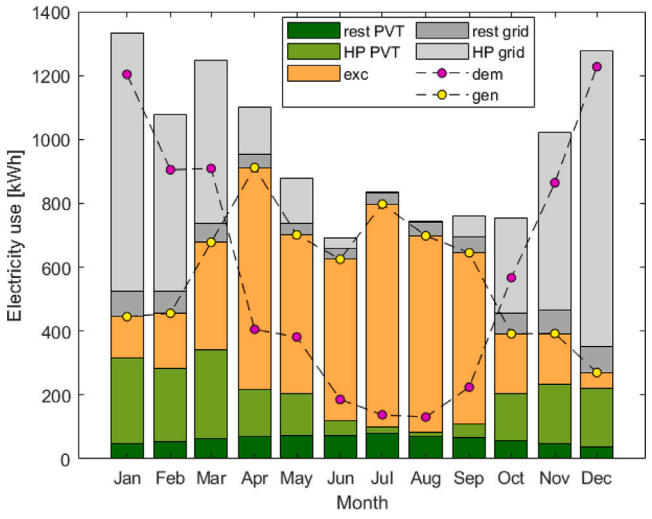

Fig. 11. Electricity use on monthly scale, depicting, generated electricity (gen) and electricity demand (dem), solar sourced electricity going to, the appliances ($rest\ PVT$), and to the HP ($HP\ PVT$), as well as the excess (exc), the grid electricity used for the appliances ($rest\ grid$) and for the HP ($HP\ grid$).

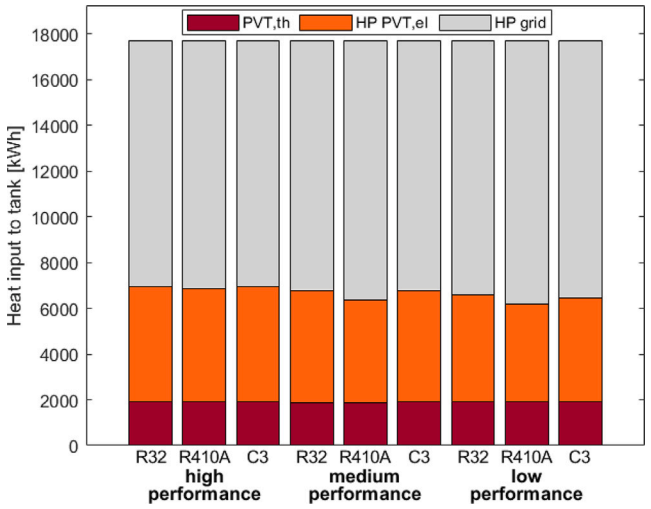

Fig. 12. Annual comparison of heat demand coverage from nine selected HP designs, three different performance levels for three different refrigerants (C3 represents propane), depicting solar thermal energy (PVT,th), solar sourced electricity going to the HP ($HP\ PVT,el$), the grid electricity used for the HP ($HP\ grid$).

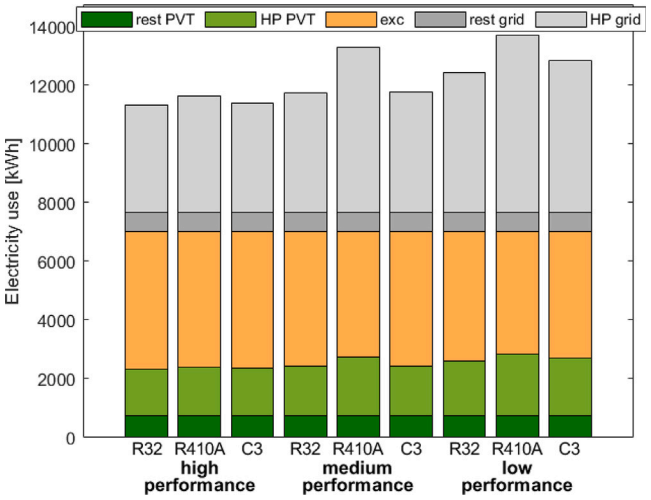

Fig. 13. Annual comparison of electricity use from nine selected HP designs, three different performance levels for three different refrigerants (C3 represents propane), depicting the appliances ($rest\ PVT$), and to the HP ($HP\ PVT$), as well as the excess (exc), the grid electricity used for the appliances ($rest\ grid$) and for the HP ($HP\ grid$).

rules on ozone-depleting refrigerants getting stricter, it would be more reasonable financially to invest in the more environmentally friendly options.

4. Comparison of different heating technologies

The comparison of the heating technologies focuses on an economic perspective. The most comparable metric identified is the $LCOE_{\mathrm{eq,el}}$, as it accounts for both electricity and heat generation and consumption as well as the investment costs, meaning that the advantages of solar generation offered by the SAHP are considered without disregarding its higher investment cost. For the standalone HP and boiler systems, the total household electricity consumption is completely covered by grid, and is also considered in the $LCOE_{\mathrm{eq,el}}$. In the recent context of the increase in energy prices, it is of particular interest to study the sensitivity of the $LCOE_{\mathrm{eq,el}}$ of different heating systems to the variation in natural gas and electricity prices. The variation of the $LCOE_{\mathrm{eq,el}}$ as a function of energy prices for each individual heating system is described in Fig. 14 for the three heating technologies.

The SAHP in Fig. 14(a) shows the lowest $LCOE_{\mathrm{eq,el}}$ for most energy price combinations, with values continuously staying between 0.2 and 0.4 Euro/kWh. The standalone HP is more sensitive to the electricity prices compared to the SAHP since it consumes more electricity. The $LCOE_{\mathrm{eq,el}}$ for the HP in Fig. 14(c) varies from 0.2–0.5 Euro/kWh on the studied interval. Only the standalone boiler, in Fig. 14(b), is affected by changing the natural gas price. All of its heating is based on natural gas while all of the electricity consumption from appliances are covered by the grid. The heating demand is bigger than the electricity demand, which explains why the effect of varying natural gas price is more important than that of the varying electricity price. The standalone boiler shows the largest variation in $LCOE_{\mathrm{eq,el}}$ over the studied interval with values varying between 0.2 and 0.6 Euro/kWh.

Fig. 15 shows which technology has the lowest $LCOE_{\mathrm{eq,el}}$ for each natural gas and electricity price combination. The natural gas and

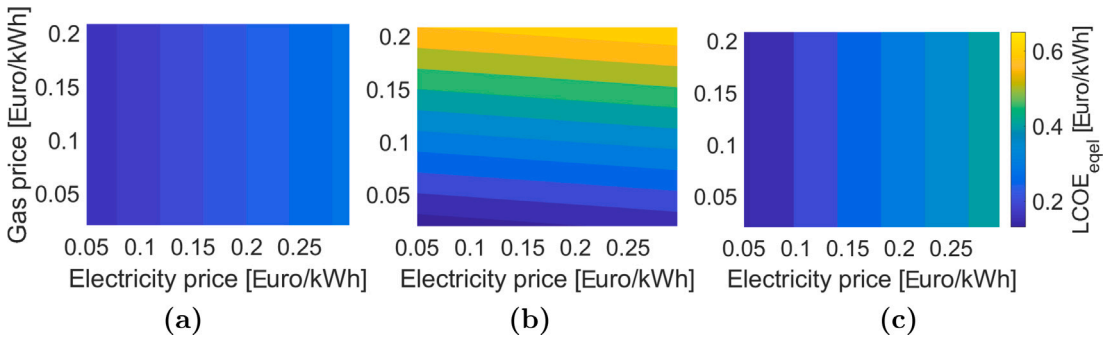

Fig. 14. $LCOE_{\mathrm{eq,el}}$ as a function of electricity and natural gas price for: (a) the SAHP, (b) standalone boiler, and (c) standalone HP.

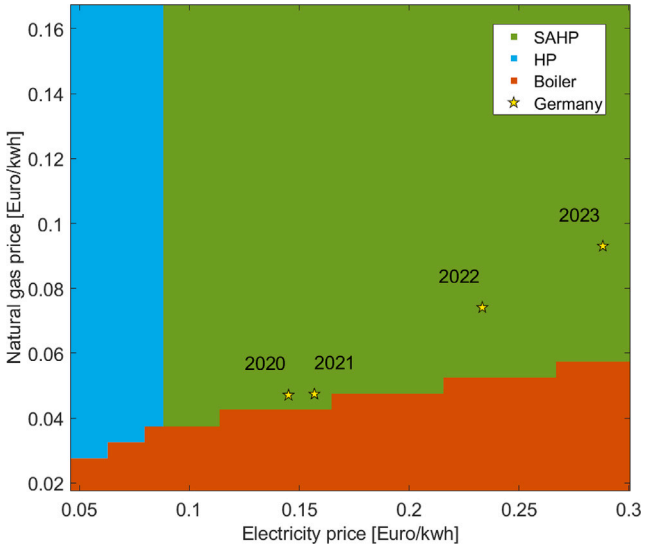

Fig. 15. Fields representing which technology has the lowest $LCOE_{\mathrm{eq,el}}$ at various natural gas and electricity prices.

electricity prices are plotted for the last four years, values are from the end of the year. The SAHP is the most cost-effective choice for most energy price combinations in the studied range. For the boiler, it is observed that increasing the electricity price allows a larger natural gas price to be tolerated while maintaining the lowest $LCOE\mathrm{eq,el}$. The boiler was almost the best option before energy prices began climbing in 2020. At electricity prices below 0.09 Euro/kWh, the standalone HP also becomes a viable option since the advantages of saving grid electricity usage become less significant in this case, and solar solutions becomes less interesting.

Even if the SAHP shows good $LCOE_{\mathrm{eq,el}}$ values, PVT collectors possess a cost barrier especially in comparison to PV panels. However, certain concepts could make PVT collectors more attractive: newer, cheaper or more efficient PVT collector technologies, incentives in the form of subsidies for PVT collector (since they reduce grid-sourced electricity consumption), and lower water tank temperatures (making it easier to produce usable solar thermal output during colder periods).

5. Limitations

The limitations of this research highlight the need for further studies on the topics discussed. They are summarized as follows:

- A single-node thermal storage model is used, assuming no spatial temperature gradients within the water tank, thereby disregarding potential performance improvements from stratified operation [64].
- Pure water is considered as the solar HTF, instead of an antifreeze solution. If the temperature of the HTF reaches below 0 °C, the options are to empty the collectors of water which, in contrast to antifreeze solutions, is harmless to the sewage system, or to heat the collectors with the water tank [22].
- Electrical energy storage is not considered; only immediate power demands are met by the generated solar power. While this simplifies the system, it does not optimize household solar electricity consumption.
- Control equipment is considered only from an economic perspective. Given the technical maturity of PVT and HP systems, the proposed control strategy is assumed to be practical.
- Risks related to sensitive loads and the reliability of electrical power, particularly concerning the HP and household appliances, are outside the study's scope.

6. Conclusions

In this study, a parallel IDX SAHP system was investigated from thermodynamic, economic, and environmental perspectives, for a typical single-family house in Germany. The proposed system involved the integration of PVT collectors and a HP, operating in parallel, to cover space heating and hot water demand. The HP and the household appliance electricity demand were partially covered by the PVT modules. The methodology involved developing a transient mathematical model for a SAHP by integrating a PVT model with HP performance maps based on various designs generated from a separate model. The performance of the SAHP was simulated using estimated household energy demand data and actual weather data from the three largest cities in Germany.

From an energy perspective, for the considered household, the system allowed over one third of the annual heat demand and around half of the annual appliance electricity demand to be covered by solar energy. However, a mismatch between solar energy generation and heat consumption limited the system's ability to utilize even larger amounts of solar energy. During summer, the low heat demand was largely met by solar energy. In contrast, during winter, the larger heat demand was primarily covered by the HP running on grid-sourced electricity. Among the cities tested, the SAHP system achieved the highest solar energy coverage in Munich (up to 39% of heat demand). Out of 54 HP designs, the high-performance design using R32 refrigerant provided the highest solar energy coverage.

Economically and environmentally, designs showing higher demand coverage by solar energy had the best performance. The high-performance HP designs using R32 and propane, were the only ones shown to be a viable investment with positive NPV (960 and 255 Euro) and PBT lower than the technology lifetime (19.3 and 19.8 years). Comparing the SAHP to other technologies, a standalone HP or natural gas boiler could only match the $LCOE_{\mathrm{eq,el}}$ of the SAHP at exceptionally low electricity or gas prices.

Germany serves as a representative case study in this work due to its temperate climate and a rapidly expanding HP market, conditions that are present in other industrialized regions. As such, the findings of this study can be reasonably extrapolated to other Central European countries with similar climatic and economic profiles, such as Austria, Switzerland, the Netherlands, and parts of France. Beyond Central Europe, the results also hold relevance for regions outside Europe that share comparable climate zones and energy market structures, including parts of North America, East Asia and Oceania. To support broad applicability, the comparison of heating technologies in this work was conducted across a wide range of energy prices, reflecting diverse global economic conditions. The analyses presented are based on variable input parameters, allowing for meaningful comparisons across multiple regional contexts. In addition, the underlying modeling approach is adaptable, as it incorporates flexible parameterization, such as energy pricing, climatic data, and policy incentives, making it a valuable framework for researchers and policymakers worldwide seeking to evaluate the performance and viability of SAHP systems under other regional conditions.

An important challenge for the parallel IDX configuration investigated in this paper, was that the increase in tank temperature by the ST loop hindered the operation of the HP using solar-sourced electricity. Elevated tank temperatures also reduced the thermal efficiency of the PVT collectors. Future work should aim to lower the HP hot-sink temperature to help mitigate these issues. Further research opportunities also include the integration of defrosting strategies and electrical energy storage, which could be effectively explored using dedicated transient simulation tools. The study concluded by proposing that the SAHP system holds development potential that could enhance its attractiveness.

CRediT authorship contribution statement

Hugo Arnesson: Writing – original draft, Visualization, Software, Investigation, Formal analysis, Data curation. **Andreas V. Olympios:** Writing – review & editing, Visualization, Software, Resources, Data curation. **Asmaa A. Harraz:** Writing – review & editing, Supervision, Software, Methodology. **Jingyuan Xu:** Writing – review & editing, Visualization, Supervision, Project administration, Methodology, Funding acquisition, Conceptualization.

Declaration of competing interest

The authors declare that they have no known competing financial interests or personal relationships that could have appeared to influence the work reported in this paper.

Acknowledgement

The authors gratefully acknowledge the support provided by the Carl-Zeiss-Stiftung, the Baden-Württemberg Stiftung, the Hector Fellow Academy, and the Klaus Tschira Stiftung.

Appendix A. Complementary equations

A.1. Circulation pump power

The PVT circulation pump power consumption is given by Eq. (A.1) [65,66]:

$$P_{\text{pump}} = \frac{\dot{m}(\Delta P_{\text{collector}} + \Delta P_{\text{PVT}})}{\eta_{\text{pump}}\rho_{\text{water}}}, \tag{A.1}$$

where $\dot{m}$ is the total mass flow rate, $\Delta P_{\text{collectors}}$ is the pressure drop in PVT collectors, set to $0.18 \cdot 10^5$ Pa, ΔP_{PVT} is the pressure drop in PVT circulation loop, η_{pump} is the pump efficiency, set to 85%, and ρ_{water} is the density of water [67].

The pressure drops in the circulation loop is given by the Darcy–Weisbach equation, see Eq. (A.2) [68]:

$$\Delta P_{\text{PVT}} = \frac{f L_{\text{pipe}}}{D_{\text{h}}} 0.5\rho \left(\frac{\dot{m}}{\rho A_{\text{pipe}}}\right)^2, \tag{A.2}$$

where f is the friction factor, L_{pipe} is the length of the pipes in the loop system, D_{h} is the hydraulic diameter of the pipes, and A_{pipe} is the internal area of the pipe system.

A.2. Overall heat transfer

The overall heat transfer coefficient through the tank is obtained by assuming that a wool insulation layer consists the main thermal resistance to heat transfer through the tank and that the thermal resistance through convection both in and outside of the tank is negligible in comparison. Eqs. (A.3) and (A.4) summarize the corresponding calculations:

$$U_{\text{ins}} = \frac{1}{R_{\text{ins}} A_{\text{WT}}}, \tag{A.3}$$

where R_{ins} is the thermal resistance of the insulation calculated for a cylindrical layer as in Eq. (A.4):

$$R_{\text{ins}} = \frac{ln\left(\frac{r_{\text{e}}}{r_{\text{i}}}\right)}{2\pi k H_{\text{i}}}, \tag{A.4}$$

where r_{e} is the external radius of tank, r_{i} is the internal radius of tank, k is the thermal conductivity set to 0.038 W/m K [69], and H_{i} is the internal height of the tank.

Appendix B. Heat pump design

The motivations for the choices of the six design conditions are described as follows:

1. Cold-source design temperature:
   This temperature corresponds to the lowest air temperature that the HP should be able to handle. The dry-bulb temperature that was exceeded 99% of the time in 2021, as recorded by meteorological stations in the three studied cities was used as the basis for cold-source design temperature [70].
2. Hot-sink/tank temperature:
   This temperature corresponds to the tank temperature. The water storage tank was used both for SHD and HWD and the tank temperature needs to satisfy conditions for both. A tank temperature of 55 °C was assumed to be sufficient to cover both SHD, which has a setpoint temperature of 50 °C, and HWD, which has a setpoint temperature of 45 °C. The HP will not be as efficient, and the COP map will no longer be valid, if the tank temperature deviates to much from the hot-sink temperature. Therefore, an upper limit was set to 65 °C, above which the HP no longer provides heat [71,72].
3. Heat output:
   The design heat output of a HP measures its size and power, serving as a proxy for its cost. An increase in heat output correlates with higher costs, yet it can also correspond to a lower specific cost per kWh. Two design heat outputs were selected. Based on the hourly heat demand load profile, a worst-case scenario was identified, corresponding to the highest observed hourly heat demand over the year [45]. This peak demand was slightly rounded down, by a few hundred W, to 5.5 kW to align with a standard HP capacity and to prevent excessive oversizing. This capacity was used as the base HP configuration. A second size of 7 kW was selected to investigate the effect of HP oversizing and its implications for thermal energy storage and flexibility.

Table B.1
Design condition combinations, selected designs are highlighted in gray.

Refrigerant	Design Temp. (°C)	PPTD (°C)	Heat output (W)	Mean COP	Tot. price (Euro)
R32	−9.2	3	5500	3.15	5119.4
			7000	3.13	5184.6
		5	5500	2.88	4979.5
			7000	2.89	4999.2
		10	5500	2.44	4815.2
			7000	2.41	4859.0
	−8.3	3	5500	3.12	5117.0
			7000	3.13	5178.5
		5	5500	2.89	4971.4
			7000	2.89	4991.2
		10	5500	2.46	4806.0
			7000	2.41	4859.6
	−6.1	3	5500	3.12	4976.6
			7000	3.13	5147.9
		5	5500	2.86	4931.1
			7000	2.90	4972.0
		10	5500	2.47	4783.6
			7000	2.41	4826.7
R410a mix	−9.2	3	5500	2.93	5039.3
			7000	2.97	5327.7
		5	5500	2.10	4874.1
			7000	2.21	5109.0
		10	5500	2.06	4743.6
			7000	1.99	4931.3
	−8.3	3	5500	2.93	5034.3
			7000	2.97	5323.5
		5	5500	2.20	4868.6
			7000	2.20	5103.8
		10	5500	2.02	4734.6
			7000	2.02	4922.0
	−6.1	3	5500	2.93	5021.0
			7000	2.97	5312.2
		5	5500	2.23	4853.8
			7000	2.16	5089.2
		10	5500	2.00	4711.9
			7000	2.06	4898.2
Propane	−9.2	3	5500	3.10	5332.7
			7000	3.09	5672.5
		5	5500	2.84	5158.9
			7000	2.83	5428.9
		10	5500	2.25	5014.5
			7000	2.25	5217.0
	−8.3	3	5500	3.10	5323.4
			7000	3.09	5666.3
		5	5500	2.84	5148.4
			7000	2.83	5420.3
		10	5500	2.25	5004.0
			7000	2.25	5209.0
	−6.1	3	5500	3.09	5300.3
			7000	3.10	5650.0
		5	5500	2.83	5122.1
			7000	2.83	5398.1
		10	5500	2.25	4977.9
			7000	2.25	5186.9

4. PPTD:
   The PPTD functions as a measure of the size of the HP HEXs, the smaller the PPTD, the larger the HEXs, and the higher the costs. The considered HEXs in this model include the evaporator and the condenser, with an equal PPTD assumed for both. It is acknowledged that while this a widely used modeling simplification that can still provide accurate system-level results, it does not necessarily reflect all real-world HP cycles. A value of 5 °C is commonly assumed. However, a PPTD of 3 °C and 10 °C are also tested for to observe the effects on costs and COP [73].
5. Refrigerant:
   Refrigerants are notorious for their high global warming and ozone depletion potentials (GWP and ODP). The choice of refrigerant is relevant when it comes to limiting the environmental impact of HPs. In this study, the refrigerants R32, R410 A and propane are considered. R410 A is a prevalent refrigerant mix in the existing HP stock with a relatively low ODP. It has a lower density than its predecessors allowing for a more compact HP and lower costs [74]. R32 is a component of the R410 A mix with a much lower GWP, which is common in newly installed HPs [75–77]. Propane has an ODP of 0 and a very low GWP. However, because of its flammable character it has been avoided in research up until recently [78].
6. Compressor type:
   The rotary-vane compressor type was assumed for all designs since they are cost-effective and function well in small-scale applications such as domestic heating.

All 54 HP designs generated and tested for in off-design are reported in Table B.1. Since the compressor type and the tank temperature are the same for every design, these parameters are not included in the table. The mean COP obtained in off-design operation and total price are given for each design. The designs selected for further analysis are highlighted in gray.

Data availability

Data will be made available on request.

References

[1] Friedrich J. World greenhouse gas emissions. World Ressources Institute; 2022, https://www.wri.org/data/world-greenhouse-gas-emissions-2019.

[2] Borgen H, Iliceto A, Christos D, Constantinescu N, Sapountzoglou N, Theologitis I, Apostolidou N, Tzoumpas A, Drivakou K, Bachoumis A. Study on power and heat sectors interactions and synergies. ENTSO-E aisbl, https://eepublicdownloads.blob.core.windows.net/public-cdn-container/clean-documents/Publications/Position%20papers%20and,%20reports/2023/entso-e_integration_power2heat_230130.pdf.

[3] Delmastro C, Chen O. Buildings. International Energy Agency; 2023, https://www.iea.org/energy-system/buildings.

[4] Wang Z, Guo P, Zhang H, Yang W, Mei S. Comprehensive review on the development of SAHP for domestic hot water. Renew Sustain Energy Rev 2017;72(9):871–81. http://dx.doi.org/10.1016/j.rser.2017.01.127.

[5] Miglioli A, Aste N, Del Pero C, Leonforte F. Photovoltaic-thermal solar-assisted heat pump systems for building applications: Integration and design methods E. Energy Built Environ 2023;4(1):39–56. http://dx.doi.org/10.1016/j.enbenv.2021.07.002.

[6] Leonforte F, Del Pero C, Aste N, Miglioli A, Croci L, Besagni G. Energy assessment and monitoring of a novel photovoltaic-thermal collector designed for solar-assisted heat pump systems. IET Renew Power Gener 2020;14(13):2323–30. http://dx.doi.org/10.1049/iet-rpg.2020.0108.

[7] Rossi C, De Rosa M, Bianco V, Scarpa F, Tagliafico LA. Comparison between different photovoltaic solar-assisted heat pumps (PVT-SAHP) configurations with retrofitted photovoltaic panels. WSEAS Trans Environ Dev 2014;10(1):329–40.

[8] Sezen K, Gungor A. Comparison of solar assisted heat pump systems for heating residences: A review. Sol Energy 2023;249:424–45. http://dx.doi.org/10.1016/j.solener.2022.11.051.

[9] Abbasi B, Li S, Mwesigye A. Energy, exergy, economic, and environmental (4E) analysis of SAHP water heaters in very cold climatic conditions. Renew Energy 2024;226. http://dx.doi.org/10.1016/j.renene.2024.120391.

[10] Zhou J, Zeng C, Wang Z, Lyu W, Tang Y, Wu D, Ji W, Yuan Y. Indirect expansion solar assisted heat pump system: A review. Sustain Energy Technol Assess 2022;53. http://dx.doi.org/10.1016/j.seta.2022.102409.

[11] Lerch W, Heinz A, Heimrath R. Evaluation of combined solar thermal heat pump systems using dynamic system simulations. Energy Procedia 2014;48:598–607. http://dx.doi.org/10.1016/j.egypro.2014.02.070.

[12] Huan C, Wang F, Li S, Zhao Y, Liu L, Wang Z, Ji C. A performance comparison of serial and parallel solar-assisted heat pump heating systems in Xi'an, China. Energy Sci Eng 2019;7(4):1379–93, https://scijournals.onlinelibrary.wiley.com/doi/10.1002/ese3.357.

[13] Lu J, Tang Y, Li Z, He G. Solar heat pump configurations for water heating system in China. Renew Sustain Energy Rev 2021;187. http://dx.doi.org/10.1016/j.applthermaleng.2021.116570.

[14] Panaras G, Mathioulakis E, Belessiotis V. Investigation of the performance of a combined solar thermal heat pump hot water system. Sol Energy 2013;93:169–82. http://dx.doi.org/10.1016/j.solener.2013.03.027.

[15] Cai J, Ji J, Wang Y, Huang W. Numerical simulation and experimental validation of indirect expansion solar-assisted multi-functional heat pump. Renew Energy 2016;93:280–90. http://dx.doi.org/10.1016/j.renene.2016.02.082.

[16] Vahidhosseini SM, Rashidi S, Hsu S, Yan W, Rashidi A. Integration of solar thermal collectors and heat pumps with thermal energy storage systems for building energy demand reduction: A comprehensive review. J Energy Storage 2024;95. http://dx.doi.org/10.1016/j.est.2024.112568.

[17] Pinamonti M, Baggio P. Energy and economic optimization of solar-assisted heat pump systems with storage technologies for heating and cooling in residential buildings. Renew Energy 2020;157:90–9. http://dx.doi.org/10.1016/j.renene.2020.04.121.

[18] Verma V, Meena CS, Thangavel S, Kumar A, Choudhary T, Dwivedi G. Ground and solar assisted heat pump systems for space heating and cooling applications in the northern region of India – A study on energy and CO2 saving potential. Sustain Energy Technol Assess 2023;59. http://dx.doi.org/10.1016/j.seta.2023.103405.

[19] Emmi G, Zarrella A, De Carli M, Galgaro A. An analysis of solar assisted ground source heat pumps in cold climates. Energy Convers Manage 2015;106:660–75. http://dx.doi.org/10.1016/j.enconman.2015.10.016.

[20] Zou L, Liu Y, Yu M, Yu J. A review of solar assisted heat pump technology for drying applications. Energy 2023;283. http://dx.doi.org/10.1016/j.energy.2023.129215.

[21] Nazari MA, Rungamornrat J, Prokop L, Blazek V, Misak S, Al-Bahrani M, Ahmadi MH. An updated review on integration of solar photovoltaic modules and heat pumps towards decarbonization of buildings. Energy Sustain Dev 2023;72:230–42. http://dx.doi.org/10.1016/j.esd.2022.12.018.

[22] Solak P, Kulesza L. The calculation of the amount of energy needed to keep the solar collector absorber surface above the freezing point of water in the polish climate all year round. Procedia Eng 2016;157:285–92. http://dx.doi.org/10.1016/j.proeng.2016.08.368.

[23] International Organization for Standardization. ISO 9806:2017. 2017, https://www.iso.org/standard/67978.html.

[24] Allan J, Dehouche Z, Stankovic S, Mauricette L. Performance testing of thermal and photovoltaic thermal solar collectors. Energy Sci Eng 2015;3(4):310–26. http://dx.doi.org/10.1002/ese3.75.

[25] Duffie JA, Beckman WA. Solar engineering of thermal processes. 4th ed.. John Wiley & Sons, Inc.; 2013, http://dx.doi.org/10.1002/9781118671603.

[26] Heydenreich W, Müller B, Reise C. Describing the world with three parameters: A new approach to PV module modelling. In: Proceedings of the 23rd European photovoltaic solar energy conference & exhibition. Fraunhofer Institute for Solar Energy Systems; 2008, http://dx.doi.org/10.4229/23RDEUPVSEC2008-4DO.9.4.

[27] Jones AD, Underwood CP. A thermal model for photovoltaic systems. Sol Energy 2001;70(4):349–59. http://dx.doi.org/10.1016/S0038-092X(00)00149-3.

[28] Pino A, Pino FJ, González GMC, Navas SJ, Guerra J. PVT potential for a small-scale brewing process: A case study. Therm Sci Eng Prog 2024;53. http://dx.doi.org/10.1016/j.tsep.2024.102670.

[29] Herrando M, Ramos A, Freeman J, Zabalza I, Markides CN. Technoeconomic modelling and optimisation of solar combined heat and power systems based on flat-box PVT collectors for domestic applications. Energy Convers Manage 2018;175:67–85. http://dx.doi.org/10.1016/j.enconman.2018.07.045.

[30] Herrando M, Guarracino I, Markides CN, Zabalza I, del Amo A. Energy characterization and optimization of new heat recovery configurations in hybrid PVT systems. In: Proceeding of eurosun conference. International Solar Energy Society; 2016, https://proceedings.ises.org/?doi=10.18086%2Feurosun.2016.08.22.

[31] Herrando M, Ramos A, Zabalza I, Markides CN. A comprehensive assessment of alternative absorber-exchanger designs for hybrid PVT-water collectors. Appl Energy 2019;235:1583–602. http://dx.doi.org/10.1016/j.apenergy.2018.11.024.

[32] Zisopoulos G, Nesiadis A, Atsonios K, Nikolopoulos N, Stitou D, Coca-Ortegón A. Conceptual design and dynamic simulation of an integrated solar driven thermal system with thermochemical energy storage for heating and cooling. J Energy Storage 2021;41. http://dx.doi.org/10.1016/j.est.2021.102870.

[33] Wang K, Herrando M, Pantaleo AM, Markides CN. Technoeconomic assessments of hybrid photovoltaic-thermal vs. conventional solar-energy systems: Case studies in heat and power provision to sports centres.
[34] Glembin J, Büttner C, Steinweg J, Rockendorf G. Thermal storage tanks in high efficiency heat pump systems – Optimized installation and operation parameters. Energy Procedia 2015;73:331–40. http://dx.doi.org/10.1016/j.egypro.2015.07.700.
[35] Kuang YH, Wang RZ. Performance of a multi-functional direct-expansion solar assisted heat pump system. Sol Energy 2006;80(7):795–803. http://dx.doi.org/10.1016/j.solener.2005.06.003.
[36] Jonas D, Theis D, Meiers J, Frey G. Model-based analysis of solar thermal and heat pump systems using TRNSYS. In: Proceedings of the international conference on solar heating and cooling for buildings and industry. 2017, http://dx.doi.org/10.18086/swc.2017.33.05.
[37] RVR Energy Technology. TiSUN FS combination tanks 800/1000 litre. 2017, https://www.rvr.ie/products/tisun-fs-special-offers.
[38] Spirax Sarco. Steam engineering principles and heat transfer. 2015, https://www.spiraxsarco.com/learn-about-steam/steam-engineering-principles-and-heat-transfer/energy-consumption-of-tanks-and-vats?sc_lang=en-GB.
[39] Poppi S, Sommerfeldt N, Bales C, Madani H, Lundqvist P. Techno-economic review of solar heat pump systems for residential heating applications. Renew Sustain Energy Rev 2018;81:22–32. http://dx.doi.org/10.1016/j.rser.2017.07.041.
[40] Ucar A, Inalli M. Thermal and economical analysis of a central solar heating system with underground seasonal storage in Turkey. Renew Energy 2005;30(7):1005–19. http://dx.doi.org/10.1016/j.renene.2004.09.015.
[41] Asaee SR, Ugursal VI, Beausoleil-Morrison I. Techno-economic assessment of solar assisted heat pump system retrofit in the Canadian housing stock. Appl Energy 2017;190:439–52. http://dx.doi.org/10.1016/j.apenergy.2016.12.053.
[42] Wang K, Herrando M, Pantaleo AM, Markides CN. Technoeconomic assessments of hybrid photovoltaic-thermal vs. conventional solar-energy systems: Case studies in heat and power provision to sports centres. Appl Energy 2019;254. http://dx.doi.org/10.1016/j.apenergy.2019.113657.
[43] Urban Land Institute Europe. Carbon pricing rapidly gaining 'much needed' traction in real estate, say ULI and PwC. 2023, https://europe.uli.org/carbon-pricing-rapidly-gaining-much-needed-traction-in-real-estate-say-uli-and-pwc/.
[44] Khorasaninejad E, Hajabdollahi H. Thermo-economic and environmental optimization of solar assisted heat pump by using multi-objective particle swam algorithm. Energy 2014;72:680–90. http://dx.doi.org/10.1016/j.energy.2014.05.095.
[45] Leone DB, Pezzutto S, Callegher CZ. Static building stock analysis. Moderate; 2023, https://moderate-project.eu/wp-content/uploads/2022/08/20230531_D3.2-Static-building-stock-analysis.pdf.
[46] Open Power System Data. When2Heat heating profiles [Data set]. 2023, http://dx.doi.org/10.25832/when2heat/2023-07-27.
[47] Eurostat. Disaggregated final energy consumption in households – quantities [Data set]. 2024, https://ec.europa.eu/eurostat/databrowser/view/nrg_d_hhq_custom_10329644/default/table?lang=en.
[48] European Commission. Photovoltaic geographical information system. 2022, https://re.jrc.ec.europa.eu/pvg_tools/en/tools.html.
[49] Mainzer K, Fath K, McKenna R, Stengel J, Fichtner W, Schultmann F. A high-resolution determination of the technical potential for residential-roof-mounted photovoltaic systems in Germany. Sol Energy 2014;105:715–31. http://dx.doi.org/10.1016/j.solener.2014.04.015.
[50] Olympios AV, Aunedi M, Mersch M, Krishnaswamy A, Stollery C, Pantaleo AM, Sapin P, Strbac G, Markides CN. Delivering net-zero carbon heat: Technoeconomic and whole-system comparisons of domestic electricity- and hydrogen-driven technologies in the UK. Energy Convers Manage 262. http://dx.doi.org/10.1016/j.enconman.2022.115649.
[51] Checkatrade. How much does a new boiler cost in 2024?. 2024, https://www.checkatrade.com/blog/cost-guides/new-boiler-cost/.
[52] British Gas. Local heroes. 2024, https://www.britishgas.co.uk/local-heroes.html.
[53] Exchange Rates. British pound (GBP) to euro (EUR) exchange rate history for 2023. 2024, https://www.exchange-rates.org/exchange-rate-history/gbp-eur-2023.
[54] Eurostat. Electricity prices for household consumers - bi-annual data [Data set]. 2024, http://dx.doi.org/10.2908/NRG_PC_204.
[55] Willuhn M. Germany raises feed-in tariffs for solar up to 750 KW. PV Magazine; 2022, https://www.pv-magazine.com/2022/07/07/germany-raises-feed-in-tariffs-for-solar-up-to-750-kw/.
[56] Eurostat. Gas prices for household consumers - bi-annual data [Data set]. 2024, http://dx.doi.org/10.2908/NRG_PC_202.
[57] Eurostat. HICP - monthly data (annual rate of change) [Data set]. 2024, http://dx.doi.org/10.2908/PRC_HICP_MANR.
[58] European Commission. Reference and discount rates [Data set]. 2024, https://competition-policy.ec.europa.eu/state-aid/legislation/reference-discount-rates-and-recovery-interest-rates/reference-and-discount-rates_en.
[59] Obalanlege MA, Xu J, Markides CN, Mahmoudi Y. Techno-economic analysis of a hybrid photovoltaic-thermal solarassisted heat pump system for domestic hot water and power generation. Renew Energy 2022;196:720–36. http://dx.doi.org/10.1016/j.renene.2022.07.044.
[60] Elston J. Viessmann boiler prices, reviews, guide & more. Boiler Central; 2024, https://www.boilercentral.com/guides/viessmann-boiler-reviews-prices/.
[61] Statista. Carbon intensity of the power sector in Germany from 2000 to 2023. 2024, https://www.statista.com/statistics/1290224/carbon-intensity-power-sector-germany/.
[62] Juhrich K. CO2 emission factors for fossil fuels. German Environment Agency; 2022, https://www.umweltbundesamt.de/sites/default/files/medien/479/publikationen/cc_29-2022_emission-factors-fossil-fuels.pdf.
[63] Statista. Annual average price of European Union Emissions Trading System (EU ETS) allowances from 2020 to 2023. 2024, https://www.statista.com/statistics/1465687/average-annual-eu-ets-allowance-prices/.
[64] Fertahi SD, Jamil A, Benbassou A. Review on solar thermal stratified storage tanks (STSST): Insight on stratification studies and efficiency indicators. Sol Energy 2018;176:126–45. http://dx.doi.org/10.1016/j.solener.2018.10.028.
[65] Rogers GFC, Mayhew YR. Heat transfer and pressure loss in helically coiled tubes with turbulent flow. Int J Heat Mass Transfer 1964;7(11):1207–16. http://dx.doi.org/10.1016/0017-9310(64)90062-6.
[66] Schmidt EF. Wärmeübergang und druckverlust in rohrschlangen. Chem Ing Tech 1967;39(13):781–9. http://dx.doi.org/10.1002/cite.330391302.
[67] Herrando M, Markides CN, Hellgardt K. A UK-based assessment of hybrid PV and solar-thermal systems for domestic heating and power: System performance. Appl Energy 2014;122:288–309. http://dx.doi.org/10.1016/j.apenergy.2014.01.061.
[68] Bellos V, Nalbantis I, Tsakiris G. Friction modeling of flood flow simulations. J Hydraul Eng 2018;144(12). http://dx.doi.org/10.1061/(ASCE)HY.1943-7900.0001540.
[69] BuildingGreen. Insulation materials and their thermal properties. 2024, https://www.greenspec.co.uk/building-design/insulation-materials-thermal-properties/.
[70] American Society of Heating Refrigerating and Air-Conditioning Engineers. Ashrae climatic design conditions. 2021, https://ashrae-meteo.info/v2.0/index.php?lat=51.148&lng=-0.190&place=%27%27&wmo=037760.
[71] Elmegaard B, Ommen TS, Markussen M, Iversen J. Integration of space heating and hot water supply in low temperature district heating. Energy Build 2016;124:255–64. http://dx.doi.org/10.1016/j.enbuild.2015.09.003.
[72] Vaillant Group. What temperature should my combi boiler be set at?. 2024, https://www.vaillant.co.uk/advice/understanding-heating-technology/boilers/what-temperature-should-my-combi-boiler-be-set-at/.
[73] Cui Q, Wang C, Gao E, Zhang X. Pinch point characteristics and performance evaluation of CO2 heat pump water heater under variable working conditions. Appl Therm Eng 2022;207. http://dx.doi.org/10.1016/j.applthermaleng.2022.118208.
[74] Miglioli A, Aste N, Pero CD, Leonforte F. Photovoltaic-thermal solar-assisted heat pump systems for building applications: Integration and design methods. Energy Built Environ 2023;4(1):39–56. http://dx.doi.org/10.1016/j.enbenv.2021.07.002.
[75] Panasonic Corporation. Panasonic's guide to R32. 2016, https://www.aircon.panasonic.eu/GB_en/news/new/panasonics-guide-to-r32/.
[76] Grank UK. Understanding the benefits of R32 refrigerant in heat pumps. 2020, https://www.grantuk.com/about/blog/understanding-the-benefits-of-r32-refrigerant-in-heat-pumps/.
[77] Mars. Navigating the world of refrigerants in heat pumps: a guide for homeowners. Renewable Heating Hub; 2024, https://renewableheatinghub.co.uk/navigating-the-world-of-refrigerants-in-heat-pumps-a-guide-for-homeowners.
[78] Swegon. Propane refrigerant for heat pumps and air conditioners. 2024, https://blog.swegon.com/uk/propane-refrigerant-for-heat-pumps-and-air-conditioners.